

Bond and charge density waves in the isotropic interacting two-dimensional quarter-filled band and the insulating state proximate to organic superconductivity

S. Mazumdar¹, R. T. Clay^{1,2}, and D. K. Campbell³

¹ Department of Physics, University of Arizona, Tucson, AZ 85721

² Cooperative Excitation Project ERATO, Japan Science and Technology Corporation (JST)

³ Department of Physics, University of Illinois , Urbana, Illinois 61801

(December 2, 2024)

We report two surprising results regarding the nature of the spatial broken symmetries in the two-dimensional (2D), quarter-filled band with strong electron-electron interactions that provides a microscopic model of the 2:1 cationic organic charge transfer solids. First, in direct contradiction to the predictions of one-electron theory, we find a coexisting “bond-order and charge density wave” (BCDW) insulating ground state in the 2D rectangular lattice for *all* anisotropies, including the isotropic limit. We argue that this persistence of the BCDW in 2D is a consequence of interchain confinement of electrons due to intrachain Coulomb interactions. Second, we find that the BCDW further *coexists* with a spin-density wave (SDW) in the range of large anisotropy (small interchain coupling). Further, in contrast to the interacting half-filled band which exhibits one singlet-to-antiferromagnet (AFM) transition, in the interacting quarter-filled band there are two transitions: first, a similar singlet-to-AFM/SDW transition for large anisotropy (small interchain coupling) and second, an AFM/SDW-to-singlet transition at smaller anisotropy (large interchain coupling). We discuss how these theoretical results apply to the insulating states that are proximate to the superconducting states of 2:1 cationic charge-transfer solids (CTS). First, we show that our conclusions remain unchanged even if one assumes the conventional “effective 1/2-filled” lattice of dimer sites for these systems: the dimer lattice unconditionally dimerizes again to give the same BCDW found in the quarter-filled band. We make detailed comparisons to recent experiments in the tetramethyl-tetrathiafulvalene (TMTTF), tetramethyl-tetraselenafulvalene (TMTSF), bisethylenedithio-tetrathiafulvalene (BEDT-TTF) and bisethylenedithio-tetraselenafulvalene (BETS)-based CTS. Our theory explains the mixed charge-spin density waves observed in TMTSF and certain BEDT-TTF systems, as well as the absence of antiferromagnetism in the BETS-based systems. An important consequence of this work is the suggestion that organic superconductivity is related to the proximate Coulomb-induced BCDW, with the SDW that coexists for large anisotropies being also a consequence of the BCDW, rather than the driver of superconductivity. We argue that the quarter-filled band BCDW is related to (a) an effective 2D 1/2-filled “negative U - positive V ” model; (b) an effective 2D 1/2-filled spin-Peierls state; (c) a “paired electron” Wigner crystal; and (d) the (pinned version of) the “smectic electron” state that has recently been proposed within certain models of doped copper oxides. That all four of these models can in principle give rise to superconductivity in the weakly incommensurate regime provides further motivation for the notion that the BCDW may be driving the superconductivity in the organics.

I. INTRODUCTION

Theoretical models of strongly correlated electron systems in reduced spatial dimensions predict a wide range of possible ground states involving broken spatial symmetries, and many of these are observed in real materials. Periodic spatial modulations of the charge density, spin density, or bond-order lead, respectively, to charge density wave (CDW), spin density wave (SDW), or bond-order wave (BOW) ground states. These modulations can in general be driven by electron-phonon (e-ph) or electron-electron interactions (e-e), which in principle can either compete or cooperate with each other in creating the broken symmetries.

Over the past two decades, considerable effort in this area has focused on the 1/2-filled band “Mott-Hubbard”

semiconductor in one (1D) and two (2D) dimensions. For instance, the 1D case has been extensively studied in the context of polyacetylene^{1,2}. If one takes into account only inter-site e-ph interactions, as in the Su-Schrieffer-Heeger (SSH) model², the well-known Peierls instability leads to a “ $2k_F$ ” BOW. Since k_F (the one-electron Fermi wavevector) = $\pi\rho/2a$, where a is the lattice constant and ρ is the number of electrons per site (= 1 for the 1/2-filled band), this produces the the spatial period 2 bond alternation/dimerization of the polyacetylene chain. Detailed studies¹ have established the initially controversial result that e-e interactions can strongly enhance this BOW and shown that, in the limit of very strong on-site Coulomb interaction, the BOW instability goes smoothly into the “spin-Peierls” (SP) instability. The 1D BOW (and SP) states can exhibit long-range order at zero temperature,

since they correspond to broken discrete symmetries (relative to the uniform lattice). In the 1D case, antiferromagnetism (AFM), which corresponds to a $2k_F$ SDW, can have only algebraically decaying order, and within models involving both e-ph and e-e interactions, the potential SDW ground state does not occur, as the BOW with singlet spin coupling dominates. In the presence of intersite Coulomb interactions, and for certain relative values of the on-site and intersite interaction parameters, a CDW can be the dominant instability³. The BOW and the CDW occur in largely non-overlapping regions of the parameter space and compete against each other^{3–6}.

In 2D the situation changes, and the AFM/ $2k_F$ SDW (which can now have long-range order at zero temperature) can be the ground state. The 1/2-filled isotropic 2D case has been investigated in great detail in recent years (mostly for the case of large intrasite Hubbard interaction but zero intersite interaction)⁷, as this limiting case is known to describe the parent semiconductor compounds of copper-oxide based high temperature superconductors. The BOW instability that exists in the 1D chain is destabilized in 2D by the Coulomb interaction^{8–10}, leading to the dominance of the $2k_F$ commensurate SDW⁷. Very recently, it has been demonstrated numerically that this SDW state appears for the smallest nonzero interchain hopping in weakly coupled 1/2-filled band chains¹¹, in agreement with previous renormalization group calculations^{12,13}. As in 1D⁶, there is no CDW-SDW coexistence in 2D^{8–10}.

The lack of coexistence between the BOW and SDW for the 1/2-filled band in both 1D and 2D can be readily understood at an intuitive level. Physically, the BOW requires singlet coupling between alternate pairs of nearest neighbor spins, which clearly precludes moments on individual sites. Conversely, the probability of charge-transfer to the left and to the right from any arbitrary site in the SDW are exactly equal, and therefore the SDW necessarily promotes equal bond lengths and bond orders. Further, since both the BOW and the SDW require that the site-occupancies by electrons be strictly uniform, neither the 1D BOW nor the 2D SDW will coexist with the CDW.

The so-called “ladder compounds,” consisting of a finite number of coupled 1D chains, provide a realization of systems intermediate between 1D and 2D, and these have also been extensively studied in the 1/2-filled band case¹⁴. Whether or not a given n-leg ladder system, for small n, exhibits the BOW now depends on whether n is odd or even. For even n, spin couplings between sites sharing a rung on the ladder are singlets, as a consequence of which there occurs a spin gap, and the bonds along the ladder are equal. The results obtained for the ladder systems could have been anticipated from the physics of the even versus odd S Heisenberg chains¹⁵. Thus at least for the simplest *monatomic* lattices, ground states of the 1/2-filled band are known: the BOW, CDW and SDW phases compete against one another and do not coexist, and 2D behavior emerges for the smallest

interchain electron transfer.

In contrast to the 1/2-filled band, broken symmetries in *non*-1/2-filled bands with strong e-e interactions have been investigated primarily in 1D limit^{16–20} or at most in the quasi-1D regime of weak interchain coupling²¹. This emphasis likely arises from the theoretical preconception that finite one-electron hopping between chains destroys the nesting feature that characterizes the 1D limit, leading necessarily to the restoration of the metallic phase²². A recent work has examined coupled chains in the limit of weak e-e interactions²³. The weak-coupling approximation employed in reference [23] reproduces the loss of nesting predicted within band theory. While the continuum renormalization group calculations^{16,17} predicted CDW-SDW coexistence for *incommensurate* bandfillings, early quantum Monte Carlo calculations for the 1/4-filled band failed to find this coexistence¹⁹. Many more recent numerical simulations on discrete finite systems assume the absence of coexistence between the $2k_F$ BOW, the $2k_F$ CDW and the $2k_F$ SDW that characterizes that 1/2-filled band also applies to the non-1/2-filled bands. Indeed, it is often assumed that the CDW is driven by the e-ph interactions and the SDW by e-e interactions and that their effects are competing. This assumption is made despite the result mentioned above that already in the simplest case of the 1D 1/2-filled band, e-e and e-ph interaction effects are known not to be competing but to act in a co-operative way to give the enhanced $2k_F$ BOW¹.

Recently, we have begun a systematic study of the nature of the broken symmetry ground states in the 2D 1/4-filled band on an anisotropic rectangular lattice with both e-ph and e-e interactions^{24,25}. Earlier work by us had already established the *cooperative* coexistence between the BOW and the period 4 “ $2k_F$ ” CDW in the 1D 1/4-filled band, with each broken symmetry enhancing the other, for both noninteracting²⁶ and interacting²⁷ electrons. The latter results have been subsequently confirmed by Riera and Poilblanc²⁸. In the more recent work^{24,25} we have demonstrated an apparently unique feature of the 1/4-filled band: namely, the coexistence of the BOW-CDW with the period 4 “ $2k_F$ ” SDW, giving rise to a coupled Bond-Charge-Spin density wave (BCSDW) that appears for weak interchain electron transfer between chains. Both discrete translational symmetry and continuous spin symmetry are broken in this unique ground state.

In the present paper, we extend our calculations to the full range of anisotropies, from uncoupled chains to an isotropic 2D lattice. We include both the SSH intersite phonons that drive a BOW² and the Holstein phonons that drive a CDW²⁹. We list three primary motivations for this extension²⁵. First, the co-operative coexistence between the BOW and the $2k_F$ SDW found in the 1/4-filled band for *weak* interchain transfer is exactly opposite to the competition between the $2k_F$ BOW and the $2k_F$ SDW (with the latter dominating for nonzero interchain transfer) in the 1/2-filled band. It is then im-

mediately natural to ask what the nature of the ground state is for *strong* interchain hopping of electrons in the 1/4-filled band. Second, from a more general theoretical perspective, whether or not the vanishing of density waves that is predicted by one-electron nesting ideas remains true for strongly correlated electrons is of considerable general interest. Finally, our results are likely to have relevance to experimental observations in the organic charge-transfer solids (CTS), including those that exhibit superconductivity^{30–32}.

Our investigations yield the surprising result that the coexisting Bond-Charge density wave (BCDW) persists as the ground state of the strongly correlated 1/4-filled band in 2D for *all* values of the interchain electron transfer, including the isotropic limit. We show that physically this result can be understood as a consequence of interchain confinement arising from strong intrachain Coulomb interactions^{33–35}. The SDW component of the BCSDW, on the other hand, attains a maximum amplitude at some intermediate interchain transfer, after which it typically vanishes at a critical value of the transfer (although under special circumstances, discussed in Section V, a weak SDW can also persist near the isotropic limit).

Concerning the applications of our model results to organic CTS, we should at the outset clarify several subtle and potentially confusing points, starting with two theoretical issues. As noted above, our definition of the band-filling corresponds to noninteracting electrons, so that using the standard stoichiometry of the 2:1 cationic CTS, there is one hole per two organic molecules, corresponding to a 3/4-filled band of electrons or a “1/4-filled” band of holes. Following convention (and relying on particle-hole symmetry), we call this the 1/4-filled case. In the above the bandfilling of 1/4 is defined in the usual manner: that is, each organic molecule is considered as a single site, and there is one hole per two sites. In the actual 2:1 cationic organic CTS, crystal structure effects unrelated to the low-temperature dynamic electronic and magnetic instabilities we wish to study can cause a dimerization of the lattice of organic molecules³⁶. As shown in Fig. 1(a), this dimerization leads to a gap in the single electron spectrum at $k_F = \pi/2a$, and consequently suggests using an effective 1/2-filled band model that focuses on the upper subband. In real space terms, which we will find more useful in the sequel, this approximation amounts to considering the system as a set of (tightly bound) dimers (*i.e.*, a diatomic lattice) with one electron per *dimer* site, as shown in Figure. 1(b). This approach has been widely applied^{36–40}, particularly with considerable success in the context of the magnetic field-induced spin density wave (FISDW) in 2:1 salts of TMTSF^{41,42}. Hence it is very important for us to clarify how this approach relates to our results. We will study this in detail in the body of the paper, but for now, we note the following. In this “effective 1/2-filled” conventional model, the electronic populations on the individual sites

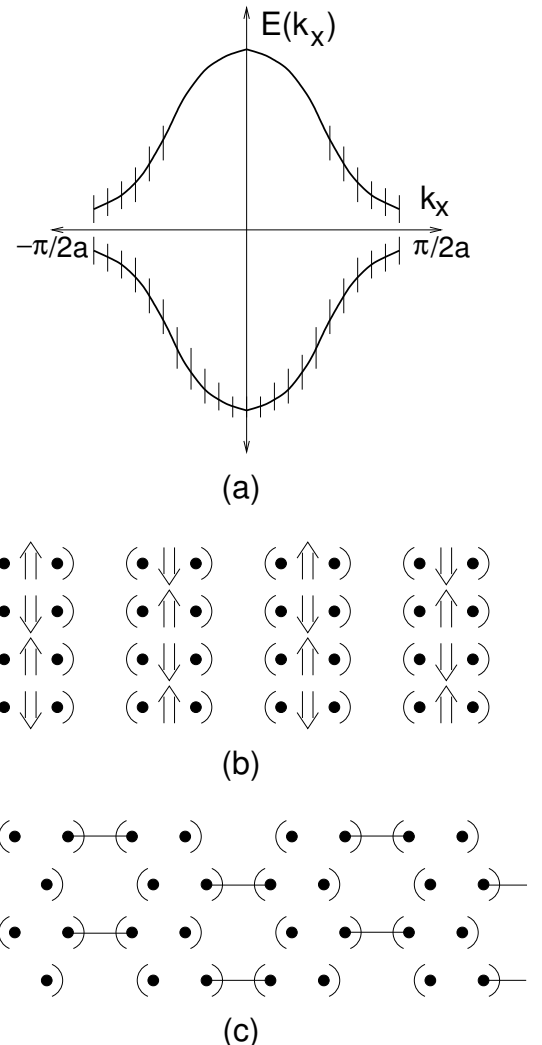


FIG. 1. The “effective” half-filled band and dimerized dimer model. (a) Dimerization in a 3/4-filled 1D band of electrons leads to a gap in the single particle spectrum at $k = \pm\pi/2a$ (a = lattice spacing), resulting in a half-filled upper subband. (b) A real space depiction of a 2D lattice of dimers in the strong correlation limit. The two sites within the parentheses form one lattice point of the dimer lattice, and the intradimer bonds are stronger than the interdimer bonds. The charge and spin populations on individual sites within each dimer are equal, and the effective 1/2-filled band lattice is antiferromagnetic in 2D. (c) Schematic of a frozen valence bond state resulting from the dimerization of dimer lattice. The interdimer bonds are now different; the line denotes a singlet bond. This frozen valence bond diagram is relevant in the 1D limit, and then again for the strongly 2D case, where the antiferromagnetism has disappeared. The antiferromagnetic phase that occurs for intermediate interchain coupling is shown in Fig. 2.

within each dimer are uniform, but strictly in the 1D limit, a *further dimerization of the 1/2-filled dimer lattice is unconditional once again*¹, as shown in Fig. 1(c). Indeed, precisely this dimerization characterizes the spin-Peierls (SP) transition observed in the nearly 1D

CTS^{24,27}, while the FISDW in the weakly 2D systems has been ascribed to the nesting instability of the effective 1/2-filled band and the “one-dimensionalization” of the 2D band in the presence of a perpendicular magnetic field. We show below the new result that this *dimerization of the dimer lattice leads spontaneously to different electronic populations on the sites within a dimer, i.e., the same period 4 “2k_F” CDW that occurs in the 1/4-filled band*. With small interchain electron transfer, the BCSDW in the “dimerized” dimer lattice will therefore have essentially the same structure as the original 1/4-filled band. Indeed, we establish explicitly below that the BCDW persists in the dimerized dimer lattice also for all interchain couplings.

Experimentally, there are also potential subtleties or confusions that we should clarify at the outset. Broadly, we expect our results to be relevant for the 1D semiconductors (TMTTF)₂X, the so-called “quasi-1D” organic superconductors (TMTSF)₂X, as well as the 2D organic superconductors (BEDT-TTF)₂X and the more recently synthesized (BETS)₂X⁴³. The lattice structure of the (TMTSF)₂X materials deviates only weakly from a rectangular lattice, but there occurs a weak dimerization along the stack axis³⁶. The interchain transfer here is also weak, and in reference [24] we showed that the highly unusual “mixed CDW-SDW state”^{36,44,45} found in (TMTTF)₂Br, (TMTSF)₂PF₆ and (TMTSF)₂AsF₆ can be explained naturally as the BCSDW state within the strongly correlated 1/4-filled band scenario. Our current work shows that dimerization of the dimer lattice leads to the same results, and hence the weak high temperature dimerization along the stack axis³⁶ is effectively irrelevant: starting from either the 1/4-filled model or the effective 1/2-filled scenario, the final outcome is the same⁴⁶. In contrast to the (TMTSF)₂X, the (BEDT-TTF)₂X occur in several different crystalline forms³¹, in several of which a strong dimerization involving nearest neighbor BEDT-TTF molecules occurs due to crystal structure effects. More importantly, the deviation from the simple rectangular lattice in some of these systems is strong. Nevertheless, we shall show below that a qualitative understanding of the broken symmetries observed in the low temperature insulating phases here can also be obtained within our picture.

As a final clarifying comment, we note that the insulator-superconductor transition in the organic CTS is often obtained under pressure, which is known to increase the interchain transfer of carriers³². This naturally leads to the question of the relation between our BCSDW and BCDW phases and superconductivity, and we explore this in some detail below. Initially, one might expect that the appearance of superconductivity coincides with the complete destruction of the background density wave due to increased interchain electron transfer. Our demonstration of the persistent BCDW, even in a region where the SDW has vanished, however, suggests a different scenario: namely, interconnected or coexisting diagonal and off-diagonal long-range order, perhaps

in the presence of a few incommensurability defects. We shall comment on this scenario, and its relation of other recent ideas regarding the origin of superconductivity in these strongly correlated systems, later.

With these comments complete, we can describe the organization of the remainder of the paper. In Section II we introduce our model Hamiltonian, as well as that of the dimerized dimer model. In Section III we present physical, intuitive arguments, based on a configuration space picture of broken symmetry^{3,8,20,27} that predict both the BCSDW for weak interchain electron transfer and the persistent BCDW state in the isotropic limit. In Sections IV and V, we present the results of extensive numerical studies, which confirm the qualitative predictions of Section III and establish both the persistence of the BCDW in the isotropic limit and the evolution of the SDW. In Section VI we discuss recent experiments that indicate the applicability of our theory to the insulating states that are proximate to the superconducting states in the organic CTS. Finally, in Section VII we summarize our conclusions and discuss a possible approach towards a microscopic theory of superconductivity in these strongly correlated electron systems.

II. MODELS AND OBSERVABLES

We consider two different extended Peierls-Hubbard Hamiltonians on a rectangular lattice 2D with (in general) anisotropic electron hopping. The first model describes a monatomic 1/4-filled band and is defined by the Hamiltonian

$$H = H_0 + H_{ee} + H_{inter} \quad (1a)$$

$$H_0 = - \sum_{j,M,\sigma} [t - \alpha(\Delta_{j,M})] B_{j,j+1,M,M,\sigma} + \beta \sum_{j,M} v_{j,M} n_{j,M} \quad (1b)$$

$$+ K_1/2 \sum_{j,M} (\Delta_{j,M})^2 + K_2/2 \sum_{j,M} v_{j,M}^2 \quad (1c)$$

$$H_{ee} = U \sum_{j,M} n_{j,M,\uparrow} n_{j,M,\downarrow} + V \sum_{j,M} n_{j,M} n_{j+1,M} \quad (1d)$$

In the above, j is a site index, M is a chain index, σ is spin, and we assume a rectangular lattice^{24,25,47}. As t_{\perp} varies from 0 to t , the electronic properties vary from 1D to 2D. An implicit parameter in the above Hamiltonian is the bandfilling, or more precisely ρ . We shall focus on the 1/4-filled case, for which $\rho = 1/2$. In applications to the organic CTS, each site is occupied by a single organic

molecule, the displacement of which from equilibrium is described by $u_{j,M}$ (with $\Delta_{j,M} = (u_{j+1,M} - u_{j,M})$); $v_{j,M}$ is an intra-molecular vibration, $n_{j,M,\sigma} = c_{j,M,\sigma}^\dagger c_{j,M,\sigma}$, $n_{j,M} = \sum_\sigma n_{j,M,\sigma}$, and $B_{j,k,L,M,\sigma} \equiv [c_{j,L,\sigma}^\dagger c_{k,M,\sigma} + h.c.]$, where $c_{j,L,\sigma}^\dagger$ is a Fermion operator. We treat the phonons in the adiabatic approximation and are interested in unconditional broken symmetry solutions that occur for e-ph couplings $(\alpha, \beta) \rightarrow 0^+$. All energies such as U , V , and t_\perp will be given in units of the undistorted intrachain hopping integral t .

The second model describes a *diatomic/dimer* lattice, with one electron per dimer. The Hamiltonian for this case is similar to that above, with identical H_{ee} and H_{inter} , but with modified intrachain one-electron term H'_0 ,

$$H'_0 = -t_1 \sum_{j,M,\sigma} B_{2j-1,2j,M,M,\sigma} - \sum_{j,M,\sigma} [t_2 - \alpha \Delta_{j,M}] B_{2j,2j+1,M,M,\sigma} + \frac{K}{2} \sum_{j,M} (\Delta_{j,M})^2 \quad (2)$$

In the above each pair of sites $(2j-1,M)$ and $(2j,M)$ forms a dimer with fixed hopping $t_1 > t$ between them, $\Delta_{j,M} = (u_{2j+1,M} - u_{2j,M})$, with $u_{2j-1,M} = u_{2j,M}$; this means that there is no modulation of the intradimer bond length, and the dimer unit is displaced as a whole. We have chosen an “in-phase” 2D arrangement of the dimer units (*i.e.*, dimers on different chains lie directly above one another, based on this configuration’s having the lowest energy, for both zero and nonzero $\Delta_{j,M}$). Notice that H'_0 does not contain the Holstein on-site e-ph coupling. Nevertheless, we will show that a site-diagonal CDW is a consequence of the BOW here.

The broken symmetries we are interested in are (i) the BOW, with periodic modulations of the intrachain *nearest neighbor* bond order $\langle \sum_\sigma B_{j,j+1,M,M,\sigma} \rangle$; (ii) the CDW, with periodic modulations of the site charge-density $\langle n_{j,M} \rangle$; and (iii) the SDW, with periodic modulations of the site spin-density $\langle n_{j,M,\uparrow} - n_{j,M,\downarrow} \rangle$. Note that in case of the dimer lattice (Eq. (2)) we are interested in both intra- and interdimer charge and spin modulations, although bond modulations can occur only between dimers. Furthermore, in the CDW and the SDW the modulations of the site-based densities occur along both longitudinal and transverse directions (though not necessarily with the same periodicities, see below). In case of the BOW, a complete description would require the determination of the phase difference between consecutive chains.

III. CONFIGURATION SPACE PICTURE OF SPATIAL BROKEN SYMMETRY

The e-e interactions in the organic CTS are comparable to the band-widths, which immediately raises questions about any perturbation theoretic approach. Even

in the strictly 1D limit, where well-established RG¹⁶ and bosonization¹⁷ techniques have existed for decades, there have recently been some surprising discoveries in the phase diagram of the extended Hubbard model^{48,49} in the *intermediate* coupling regime. In 2D, the situation is considerably more complex, and, despite some promising recent work on smectic phases⁵⁰ and novel strong coupling techniques⁵¹, there exists at present no analytic technique that can capture the physics of our Hamiltonian in 2D for intermediate coupling. Further, standard mean field theory techniques, while essential to provide some initial insight, can fail to provide reliable results, as we shall demonstrate below. Hence, much of our work perforce consists of “numerically exact” many-body computations. Since numerical work on the correlated model Hamiltonians can only be done for (fairly small) finite lattices, it is imperative that we develop a convincing physical picture of the possible spatial broken symmetries in the 1/4-filled band to guide our simulations. As we have previously noted, the one-electron band picture becomes essentially inapplicable for the case of strong U and V of relevance here: for example, band theory would predict that all broken symmetries vanish for moderate t_\perp in the 1/4-filled band, and neither the BCSDW nor the persistent BCDW would be expected within band theory. Therefore in this section we shall extend the physical picture based on “configuration space” from the previously studied 1/2-filled case^{3,8} to the 1/4-filled band, focusing on (i) the transition from 1D to 2D, and (ii) the difference from the 1/2-filled band *monatomic* lattice. Brief presentations of these physical ideas for $t_\perp = 0$ ^{26,27} and $t_\perp \ll t^2$ ²⁴ have been made previously. Here we discuss these ideas in greater detail, for the complete range $0 \leq t_\perp \leq t$.

Within the configuration space picture of broken symmetry^{3,8,20}, each broken symmetry state, independent of band-filling, can be associated with a small number of equivalent configurations that are related by the symmetry operator in question. For commensurate ρ , these configurations are easily determined by inspection. The relevant configurations consist of repeat units which themselves possess the same periodicity as the density wave. For illustration, we choose the 1D 1/2-filled band. In this case, each broken symmetry has two extreme configurations, the pairs corresponding to the SDW, BOW and CDW being, respectively: the two Néel states $\dots \uparrow\downarrow\uparrow \dots$ and $\dots \downarrow\uparrow\uparrow \dots$ (SDW); the two nearest neighbor valence bond diagrams $(1,2)(3,4)(5,6)\dots(N-1,N)$ and $(N,1)(2,3)(4,5)\dots(N-2, N-1)$ (where (i,j) is a spin singlet bond between sites i and j and N is the number of sites) (BOW); and the configurations $\dots 202020 \dots$ and $\dots 020202 \dots$ (where the numbers denote site occupancies) (CDW). N applications of the one-electron hopping term in Eq. (1) on any one extreme configuration (corresponding to a given broken symmetry) generates the other extreme configuration, but for $N \rightarrow \infty$ this mixing of configurations is small, and the ground state resembles one or the other of the extreme configurations

qualitatively, with reduced spin moment, bond order or charge-density difference due to quantum fluctuations³.

The key insight of the configuration space heuristics is that the qualitative effects of many-body Coulomb interactions, as well as additional one-electron terms, can be deduced from their effects on any one of the extreme configurations^{3,8,20}. As a trivial example of this, a repulsive Hubbard U destroys the CDW in the 1/2-filled band, simply because double occupancies “cost” prohibitively high energy. Significantly, in the 1/2-filled band, the extreme configurations favoring the SDW, the BOW and the CDW are different, and there is a complete lack of overlap between them. This essentially guarantees the absence of coexistence among these broken symmetries in both 1D and 2D.

To apply these ideas to the 1D 1/4-filled band, we begin by considering the on-site charge configurations. A $2k_F$ ($4k_F$) density wave here has period 4 (2) in configuration space. As discussed above, the extreme configurations of interest must also have period 4 or 2, and there are then only three distinct sets of extreme charge configurations. These contain the repeat units ...2000..., ...1100..., and ...1010..., respectively, where the numbers again denote site occupancies. There are four distinct configurations for sets 1 (...2000...) and 2 (...1100...), whereas there are only 2 for set 3 (...0101...). By analogy with the 1/2-filled band (see above), we now introduce spins and note that configurations belonging to sets 2 and 3 can again have spin singlet bonds between pairs of nearest neighbor singly occupied sites, or the spins of the occupied sites can alternate as in the 1/2-filled band Néel configurations. Let us now show, by considering the different cases separately, how e-e interactions affect these configurations and how an understanding of these effects suggests (correctly!) the broken symmetries to be studied.

A. 1/4-filled band, $t_{\perp} = 0$, $U = V = 0$

The non-interacting case provides a simple example to introduce some of the important differences between the 1/4-filled and 1/2-filled bands. For definiteness, we focus on the set of configurations (...2000...), which corresponds to the period 4 “ $2k_F$ ” CDW that is obtained in the $U = 0$ limit within an actual calculation²⁶. The charge densities ρ_j on the sites have the functional form

$$\rho_j = 0.5 + \rho_0 \cos(2k_F j a) = 0.5 + \rho_0 \cos(\pi j / 2) \quad (3)$$

since each ‘0’ that is immediately next to a ‘2’ is different from the other pair of sites labeled ‘0’ that are further away from the ‘2’. A very important difference from the 1/2-filled band thus follows immediately: whereas in the 1/2-filled band differences in bond-orders arise from spin-effects only (the probability of charge-transfer is greater between nearest neighbor singlet-coupled sites than between nearest neighbor non-bonded sites³), in non-1/2-filled bands this difference can also originate from site

occupancies. Within the ‘cartoon’ occupancy scheme ...2000..., for example, the probabilities of charge-transfer between a ‘2’ and the two neighboring ‘0’s are larger than that between the two neighboring ‘0’s themselves, and thus *the same extreme configuration* is also related to the period 4 “ $2k_F$ ” BOW that occurs for $U = V = 0$ but $\alpha \neq 0$ in Eq. (1)²⁶ and leads to a distortion of the lattice of the form

$$u_j = u_0 \cos(2k_F j a) = u_0 \cos(\pi j / 2), \quad (4)$$

with bonding pattern “SSWW” (for strong, strong, weak, weak), where a strong (weak) bond has hopping $t_S > t$ ($t_W < t$). *Precisely because the BOW and the CDW here are both derived from the same extreme configuration*, they coexist in the noninteracting 1/4-filled band²⁶.

B. 1/4-filled band, $t_{\perp} = 0$, $U, V > 0$

For nonzero (positive) U and V , the interplay among the various possible broken symmetries becomes both more subtle and more interesting. Since double occupancies “cost” energy, the extreme configuration ...2000... is suppressed even at a relatively small U^{27} . For the strongly correlated ($U \rightarrow \infty$) 1D 1/4-filled band with convex long range interactions, Hubbard showed that there exist *two* different Wigner crystals, with occupancy schemes ...1100... and ...1010...⁵². On first consideration, the extreme configuration ...1010..., corresponding to a period 2 “ $4k_F$ ” CDW⁵², initially appears to be strongly preferred, but in fact more careful analysis shows that it dominates the ground state only for fairly substantial V . This can be seen rigorously for $U \rightarrow \infty$, where the 1/4-filled *spinful* band can be mapped rigorously to the 1/2-filled *spinless* band⁵³, which in turn can be mapped (via a Jordan-Wigner transformation) to an anisotropic Heisenberg spin 1/2 chain⁵⁴. Using this approach, one finds that the period 2 “ $4k_F$ ” CDW becomes the ground state only for $V > V_c = 2$ (in units of $|t|$)⁵⁵. For finite U , numerical results⁵⁶ show that V_c is slightly larger than 2. Given the estimated values of V in the organic CTS, it seems unlikely that they will exhibit this (...1010...) intrachain ordering. This expectation is strongly supported by the results that the ...1010... CDW cannot coexist with the BOW^{3–6}, whereas the (TMTTF)₂X are known to exhibit a SP-BOW transition³². Hence we put aside further study of the (...1010...) order for the moment, noting only that this CDW is also obviously stable (with a π phase shift between adjacent chains) in 2D for large enough nearest neighbor Coulomb repulsion.

For $V < V_c$ the extended 1D Hubbard model at 1/4-filling is a Luttinger liquid⁵⁷ that is also susceptible to a $2k_F$ bond and charge distortion, and it is this distortion that can be described by any one of the four equivalent configurations ...1100...²⁷. The $2k_F$ CDW now has the form

$$\begin{aligned}\rho_c(j) &= 0.5 + \rho_0 \cos(2k_F ja - 3\pi/4) \\ &= 0.5 + \rho_0 \cos(\pi j/2 - 3\pi/4),\end{aligned}\quad (5)$$

and also coexists with BOW, since the charge-transfer across a ‘1 – 1’ bond is different from that across a ‘1 – 0’ (or ‘0 – 1’) bond, which again is different from the charge-transfer across a ‘0 – 0’ bond. It is a subtle but crucial fact, confirmed by earlier numerical studies²⁷, that this same CDW can now promote *two* different BOWs, each with three different bond strengths. In each of these the ‘0 – 0’ bond is the weakest, but depending upon the strength of the Coulomb interaction, the ‘1 – 1’ bond can be stronger than a ‘1 – 0’ (or ‘0 – 1’) bond (since charge-transfer in the former can occur in both directions), but it can also be weaker (since charge-transfer in the former leads to double occupancy, while no double occupancy is created in the charge transfer between a ‘1’ and a ‘0’). Consistent with this and the numerical results²⁷, we shall refer to the first bonding pattern as “SUWU” (for strong, undistorted, weak, undistorted), where a strong bond has $t_S > t$, an undistorted bond has $t_U = t$, and a weak bond has $t_W < t$. This BOW has pure period 4 “ $2k_F$ ” periodicity and is accompanied by lattice distortion

$$u_j = u_0 \cos(2k_F ja - \pi/4) = u_0 \cos(\pi j/2 - \pi/4). \quad (6)$$

Again consistent with the numerical results we call the second bonding pattern “W’SWS” (for a stronger weak bond, strong, weak, strong, with $t_S > t > t_W > t_W'$). Interestingly, the W’SWS bonding pattern is a superposition of the pure $2k_F$ period 4 SUWU structure and the pure $4k_F$ period 2 SWSW structure and is accompanied by lattice distortion

$$\begin{aligned}u_j &= u_0[r_{2k_F} \cos(2k_F ja - \pi/4) + r_{4k_F} \cos(4k_F ja)] \\ &= u_0[r_{2k_F} \cos(\pi j/2 - \pi/4) + r_{4k_F} \cos(\pi j)],\end{aligned}\quad (7)$$

where r_{2k_F} and r_{4k_F} are the relative weights of the $2k_F$ and $4k_F$ bond distortions, respectively²⁷. These results were established numerically in reference [27], where from comparisons to available experimental data in the 1:2 anionic TCNQ systems it was also shown that the phase relationship between the coexisting $2k_F$ CDW and the W’SWS BOW (the W’ bond connects sites with greater charge densities than the W bond) is precisely in agreement with theory.

Very importantly, we show below that the dimerization of the dimer lattice with one electron per dimer also leads to a W’SWS bonding pattern (see Fig. 1(c)), which in its turn promotes the site occupancy scheme ...1100.... This coexistence will therefore occur in either the full 1/4-filled band model or the effective 1/2-filled, dimerized dimer approach.

C. 1/4-filled band, $t_\perp \ll t, U, V \neq 0$.

The above two BOW-CDWs describe the ground state of the interacting 1/4-filled band in the limit of $t_\perp = 0$,

where the ‘1 - 1’ bond is a singlet. As in the 1/2-filled band though, singlets may be anticipated to give way to SDW order for $t_\perp \neq 0$. Thus we must understand the role of the spin degrees of freedom. Once specific spins are assigned to the sites labeled ‘1’ in the ...1100... configuration, the sites labeled ‘0’ become distinguishable, as a given ‘0’ site is now closer to one particular ‘1’ (up or down) than the other²⁴. In this case the ‘0’ site is expected to acquire the spin characteristic of its neighboring ‘1’. The charge and spin along a chain can now thus be denoted as $\uparrow, \downarrow, \downarrow, \uparrow$, where the sizes of the arrows are schematic measures of the charge and spin densities on the sites. Note that this represents the SDW of the form

$$\begin{aligned}\rho_s(j) &\equiv \langle c_{j,M,\uparrow}^\dagger c_{j,M,\uparrow} - c_{j,M,\downarrow}^\dagger c_{j,M,\downarrow} \rangle \\ &= \rho_{s2k_F} \cos(2k_F ja - \pi/4) + \rho_{s4k_F} \cos(4k_F ja - \pi),\end{aligned}\quad (8)$$

which *coexists* with the BOW and CDW.

Commensurability effects imply that the possible phase shifts between adjacent chains in the anisotropic 2D system are 0, $\pi/2$ and π , and we have performed explicit numerical calculations to determine that the lowest energy state is obtained with a phase shift of π . The intrachain bond orders, determined by the probabilities of nearest neighbor charge-transfers, continue to be different for the different pairs of neighboring sites. This is the major difference between the possible broken symmetries in the 1/2-filled and 1/4-filled band. While in the 1/2-filled band there is no overlap between the extreme configurations favoring the BOW, CDW and SDW, in the weakly 2D 1/4-filled band *the same extreme configuration supports all three broken symmetries*²⁴. For small nonzero t_\perp we therefore expect a strong co-operative co-existence between the BOW, the CDW and the SDW. Furthermore, since the same CDW coexists with both the SUWU BOW and the W’SWS BOW, this coexistence is independent of which particular BOW dominates. This has been explicitly demonstrated in reference [24], where it was shown that the overall ground state for small t_\perp is one of the two BCSDW states shown in Fig. 2, with overall 2D periodicity of $(2k_F, \pi)$.

D. 1/4-filled band, $t_\perp \leq t, U, V \neq 0$.

What happens as t_\perp is further increased? Within k -space single-particle theory, increasing t_\perp should destroy the nesting of the Fermi surface. But as we have indicated above, our real space analysis predicts, and our numerical results will establish, that this destruction does not occur. To argue this convincingly, we must first show how this destruction of the nesting, which certainly does occur for non-interacting electrons, can be correctly described within our configuration space picture of the broken symmetry. Recall that the one-electron hopping term in Eq. (1) introduces “paths” between the extreme configurations, where each step in a given path connects two

configurations related by a single hop^{3,8,20}. Nonzero t_{\perp} introduces many additional paths connecting the extreme configurations that are the 2D equivalents of ...1100... (with a π -phase shift between consecutive chains). For $U = V = 0$, there is no inhibition of these paths, and it therefore becomes easier to reach one extreme configuration from another, leading to enhanced configuration mixing (relative to 1D), which in its turn destroys the “nesting” and the broken symmetry.

The situation described above changes, however, for nonzero Coulomb interaction. Interchain hopping t_{\perp} leads to partial double occupancy on a single site ($\uparrow\downarrow$) with an energy barrier that, while less than the bare U , is a U_{eff} that increases with U . The energy barrier to *interchain* hopping leads to “confinement” of the electrons to single chains, a concept that has been widely debated recently, in the context of high T_c superconductors^{33–35}. For large enough U_{eff} , the confinement can be strong enough that the broken symmetry state can persist up to the isotropic limit $t_{\perp} \sim t$.

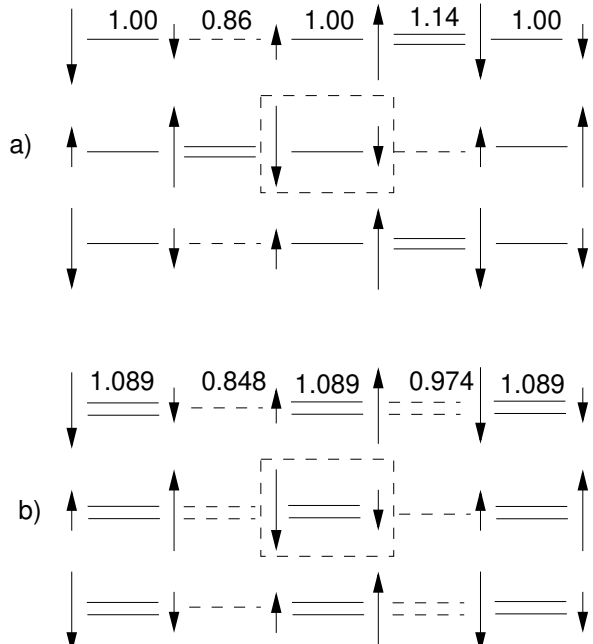


FIG. 2. Sketches of the BCSDW ground states that occur for small t_{\perp} in the strongly correlated, anisotropic 2D 1/4-filled band. The arrows indicate the spin directions and their sizes indicate the relative charge and spin densities. The hopping integrals used to calculate the energies of the distorted lattices correspond to (a) $r_{4k_F} = 0$ (see text, Section V) and (b) $r_{4k_F} = r_{2k_F}$, and are shown above the bonds along the top chain. This variation in t reflects the BOW. The bond-distortion pattern in (b), with slightly modified weak bond hopping integrals, also corresponds to the dimerized dimer lattice for small enough t_{\perp} . Note that the charge ordering corresponds to the 1D paired electron crystal along the longitudinal *and* both diagonal directions and the monatomic Wigner crystal along the transverse direction.

More precisely, the bond and charge components of the

BCSDW can persist up to the isotropic limit $t_{\perp} \sim t$, leading to the BCDW state we have previously introduced. The evolution of the spin structure is different from and more subtle than the bond and charge components. From the cartoons in Fig. 2, we see that for the SDW to exist it is essential that the ‘0’s have a spin “direction”. In the small t_{\perp} case, the sign of the spin on a ‘0’ is necessarily that of the nearest *intrachain* ‘1’. Note, however, that each ‘0’ also has two *interchain* ‘1’s as neighbors and that for a stable SDW, the spin densities of the ‘1’s that are neighbors of a specific ‘0’ must be opposite (as shown in the Figure). Therefore, with increasing t_{\perp} , competing effects occur. On the one hand, the magnitude of the interchain exchange coupling $J_{\perp} \sim t_{\perp}^2/U_{eff}$ increases. On the other hand, the spin density on a site labeled ‘0’ decreases because of the canceling effects of the *intra*- and *inter*-chain neighboring ‘1’s. We thus expect the SDW of the 2D lattice to vanish at a t_{\perp}^c that will depend on the magnitudes of the bare U and V .

This description of the evolution of the SDW applies to the true 1/4-filled band. In lattices that are dimerized initially, further dimerization leads to the occupancy ‘10’ or ‘01’ on each dimer. If the original dimerization is very strong, the spin on a given ‘0’ will continue to be strongly influenced by the spin on its partner in the dimer, and t_{\perp}^c at which the SDW vanishes in this case will be larger.

The above conclusions regarding the persistence of a BCDW even in the isotropic 2D interacting 1/4-filled lattice differ not only qualitatively from the single particle nesting ideas that predict the vanishing of the broken symmetry, but also from the results for the interacting 1/2-filled band, in which the SDW dominates in 2D over the BOW. The robustness of the BCSDW and the BCDW relative to the uniform metallic state can be understood from the cartoon occupancy schemes in Fig. 2. It is instructive to discuss the BCDW state in terms of the two large U Wigner crystal structures discussed by Hubbard⁵². We refer to the ...1100... electron arrangement as that of a “paired electron crystal”, and the ..1010... as the “monatomic Wigner crystal.” For the 3D low density electron gas, Mouloupoulos and Ashcroft⁵⁸ showed that there exists an intermediate density range where the paired electron crystal has lower energy than the monatomic Wigner crystal, and the region $0 < V < V_c$ in our discrete lattice case can be thought of as intermediate between the $V = 0$ and $V > V_c$. A striking feature of the BCSDW and the BCDW occupancy scheme is that it is a paired electron crystal along the chains (...1100..., periodicity $2k_F$), a monatomic Wigner crystal transverse to the chains (...1010..., periodicity $4k_F$), as well as a paired electron crystal along both diagonals (...1100..., periodicity $2k_F$). It is thus possible to predict that even in the presence of interactions not explicitly included in Eq. (1), the BCDW continues to persist. For instance, by enhancing the $4k_F$ charge ordering along the transverse direction, the nearest neighbor interchain Coulomb interaction V_{\perp} will further enhance the stability of the BCDW. Similarly, the diagonal

...1100... charge ordering implies that even the additions of hopping t_{diag} and Coulomb repulsion V_{diag} along the diagonals will not destroy the BCDW state for realistic parameters: in particular, V_{diag} stabilizes the BCDW relative to the other Wigner crystal (...1010...) along both x and y directions.

We focus our final remarks in this qualitative discussion on the stability of the BCDW over the SDW in the 1/4-filled band. This seemingly counterintuitive (at least based on our experience with the insulator-insulator transition in 1/2-filled systems) result can be understood from a variational standpoint by considering the competition between the double dimerization of the $\rho = 1/2$ dimer lattice and the SDW of the undistorted dimer lattice. Our arguments here are heuristic and the goal is to point out the difference between $\rho = 1/2$ and $\rho = 1$ insulators at the simplest level. We consider only the simple Hubbard Hamiltonian with $V = 0$ (since for $\rho = 1/2$ the periodicity of the CDW is the same for all $V < V_c$ and while for $\rho = 1$ the V merely reduces the effective on-site correlation). For completeness we repeat the variational argument for the dominance of the SDW over the BOW in $\rho = 1$. Consider the Heisenberg antiferromagnetic spin Hamiltonian

$$H = J \sum_{\langle ij \rangle} S_i \cdot S_j \quad (9)$$

Consider also the singlet variational state (1,2)(3,4)....(N-1,N), with singlet bonds between nearest neighbors in 1D and the Néel state $\dots \uparrow\downarrow\uparrow\downarrow \dots$. The energy of an isolated singlet bond is $-(3/4)J$ while that of a 2-site Néel state is $-(1/4)J$. The overall variational energy of the singlet state in 1D is $-(3/8)NJ$ and that of the Néel state $-(1/4)NJ$, so that the singlet dominates over the Néel state in 1D. In the 2D isotropic $N \times N$ lattice, we compare (1) the frozen valence bond state in which each chain still has the same spin couplings as in 1D (note that at the level of our approximation the relative phases between consecutive chains make no difference), and (2) the 2D Néel state. The variational energy of the frozen valence bond state is $-(3/8)N^2J$, but now because of the larger number of nearest neighbors the energy of the Néel state has a lower value $-(1/2)N^2J$, which therefore dominates over the frozen valence bond state. Thus for $\rho = 1$ in 1D the SP state dominates, while in 2D the SDW wins over the SP state. While this argument may appear simplistic, it nevertheless motivates the result we observe in our simulations.

Consider now the isotropic 2D *dimerized* $\rho = 1/2$ lattice with moderately strong dimerization. The effective 1/2-filled band is clearly a SDW, with the dimerization pattern being necessarily “in-phase” between consecutive chains, as shown in Fig. 1(b) (to prevent confusion in what follows we have not shown the bonds in Fig. 1(b), but it is understood that the spin couplings between the two sites within each parenthesis is larger than the interdimer spin couplings, and the interdimer spin-couplings

are equal in the SDW). The individual site populations are equal in this state and each is exactly 1/2. Our contention is that this state has a *higher* variational energy than that reached by further dimerization of the dimer lattice, which gives the $\rho = 1/2$ frozen valence bond state shown in Fig. 1(c), where there occur interdimer singlet bonds and site occupancies ...1100... (the singlet bonds in Fig. 1(c) are between the “occupied” sites). The reason for this is that unlike in $\rho = 1$, the exchange integrals that describe the effective Heisenberg models in the SDW and the singlet are now *different*, in spite of the fact that both Heisenberg systems are derived from the same Hubbard Hamiltonian. In Fig. 1(c), we are considering isolated singlet bonds, with site occupancies of 1, and J is clearly $2t^2/U$, exactly as for $\rho = 1$. In Fig. 1(b), on the other hand, the exchange integral has to correspond to a true $\rho = 1/2$ system, since each site occupancy is now 1/2. The exchange integral J' for arbitrary ρ in 1D is $2(t^2/U)\rho[1 - \sin(2\pi\rho/2\pi\rho)]^{53}$, so that for $\rho = 1/2$ we have $J' = (1/2)J$ along each chain (the x-direction). This expression is strictly true only in the 1D undistorted chain, and for the distorted 1D chain or in 2D one needs to calculate J' from comparing singlet-triplet gaps within the structure corresponding to Fig. 1(b) and within the 1/2-filled band. We have calculated these gaps for finite lattices separately for the longitudinal and transverse directions and have found that while $J' = (1/2)J$ is quite accurate for the longitudinal direction, the J' in the transverse direction is *even smaller* (the difference between the longitudinal and transverse directions originates from dimerization along the longitudinal direction only), with the restriction that only interdimer hops lead to spin exchange. Even if we consider the largest possible value for $J' = J/2$, the variational energy of the Néel state is Fig. 1(b) is then $-(1/2)(N^2/2)J' = -(1/8)N^2J$, while that of the frozen valence bond state in Fig. 1(c) (with $N^2/4$ singlet bonds) is $-(3/4)N^2/4J = -(3/16)N^2J$. Thus the frozen valence bond state dominates over the dimer SDW, implying that the dimerization of the dimer lattice is unconditional, and the difference from the simpler $\rho = 1$ case arises from the smaller (by factor of 2) exchange integral in the uniform dimer lattice of Fig. 1(b). The above approach is obviously simplistic, but no more so than the physical argument for the dominance of the SDW in $\rho = 1$. The argument is not to be considered a proof, but rather, it provides convincing physical motivation for the later numerical results establishing the dominance of the BCDW over the SDW for strong inter-chain coupling in the 1/4-filled case.

IV. NUMERICAL RESULTS IN 1D

Limitations of computational capability will compel us to use fairly small lattices in 2D and will prevent us from studying dynamical phonons (even at a classical, self-consistent level). As a consequence, we will have to

work with explicitly distorted lattices, rather than allowing the distortions to arise naturally, as they would in larger lattices calculated with dynamical phonons. To provide justification for this approach, in this section we (a) extend our previous 1D results obtained with nonzero α and β ²⁷ to zero e-ph couplings, to demonstrate that these bond and charge distortions are unconditional, and (b) show that the dimerization of the dimer lattice (see Eq. (2)) leads to the same CDW as the monatomic 1/4-filled band.

It is known that in a sufficiently long open chain the bond orders and the charge densities at the center of the chain show the behavior in the long chain limit, even in the absence of the e-ph coupling. In Fig. 3(a) we show the exact nearest neighbor bond orders and charge densities at the center of an open *undistorted* chain of 16 atoms with all hopping integrals equal, for $U = 6$, $V = 1$. Note that both the BOW and the CDW show the $2k_F$ modulations discussed in section III, and appear in spite of uniform hopping integrals.

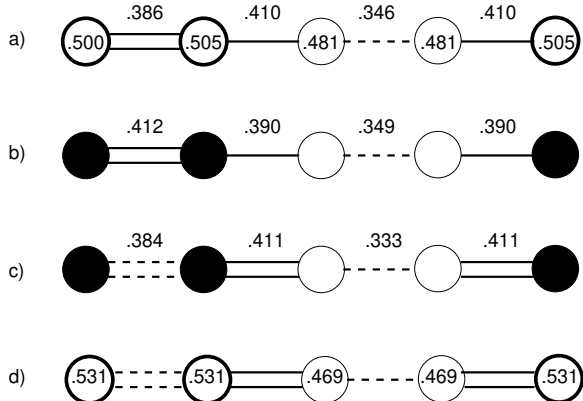


FIG. 3. Numerical results of 1D simulations for $U = 6$, $V = 1$. (a) Charge densities (numbers inside each circle, which represents one molecular site) and bond orders (numbers against the bonds) at the center of an open uniform chain of 16 sites for $\alpha = \beta = 0$. (b) Bond orders in a 16 site periodic ring with uniform hopping, and with externally imposed period 4 magnetic field of the same form as in Fig. 2, with amplitude $\epsilon = 0.05$. (c) Same as in (b) with $\epsilon = 0.1$. Because of equal bond lengths and nonzero V , there is a weak contribution by the ...1010... CDW to the ground state here and the charge densities are not pure ...1100... The filled (unfilled) circles correspond to large (small) charge densities. The bond orders also show weak deviation from pure SUSU or W'SWS behavior, and the bond orders shown are averages for each kind of bond. The magnetic field induced SDW creates a spontaneous BCDW. (c) Charge densities in a periodic dimerized dimer lattice of 16 sites. The double bond corresponds to $t = 1.2$, and the dotted and double dotted bonds to $t = 0.7$ and 0.9, respectively. Note that the CDW pattern in this effective 1/2-filled band system is the same as the 1/4-filled band lattices in (a), (b) and (c).

Second, we recall that in a purely 1D system, a LRO SDW can occur only if an external staggered magnetic

field is applied. We therefore incorporate an additional (external field-like) term

$$H_{SDW} = - \sum_j \epsilon [n_{j,\uparrow} \cos(2k_F j) + n_{j,\downarrow} \cos(2k_F j + \pi/2)] \quad (10)$$

and consider $H + H_{SDW}$ for the 1/4-filled band with amplitude $\epsilon = 0.1$. In reference [27] the same Hamiltonian was investigated for the case of finite bond distortion. Figs. 3(b) and (c) show the bond orders and CDW for a periodic ring (zero e-ph coupling and *undistorted* hopping integrals) with the SDW $\uparrow\downarrow\uparrow$ superimposed on it. Note that because of the periodicity, the bond orders are uniform for the finite ring for $\epsilon = 0$. For $\epsilon = 0.05$ (Fig. 3(b)) and 0.1 (Fig. 3(c)), the externally imposed SDW creates spontaneous BOWs with $r_{4k_F} = 0$ and $r_{4k_F} \neq 0$, respectively.

In Fig. 3(d) we show the charge densities on a *periodic* ring of 16 sites, now for the dimerized dimer lattice (the hopping integrals here are 1.2, 0.9, 1.2 and 0.7). The charge modulations (which appear entirely due to modulations of the *interdimer* bond orders) on the sites are exactly as in Figs. 3(a)–(c), with the larger charges occurring on the sites connected by the stronger weak bond (the W' bond, with $t_{W'} = 0.9$). In discussions of the spin-Peierls transition within the effective 1/2-filled band (corresponding to the dimer lattice), it is usually assumed that the electronic populations within each dimer cell remains uniform in the spin-Peierls state. Fig. 3(d) clearly shows that this is not true.

V. NUMERICAL RESULTS IN 2D

To confirm the expectations based on the qualitative arguments of Section III, we use exact diagonalization, Hartree-Fock, and Constrained Path quantum Monte Carlo (CPMC)⁵⁹ numerical techniques to calculate for representative finite 2D lattices: (i) the electronic energy gained upon bond distortion,

$$\Delta E \equiv E(0) - E(u_{j,M}), \quad (11)$$

where $E(u_{j,M})$ is the electronic energy per site with *fixed* distortion $u_{j,M}$ along the chains; (ii) the site charge densities $\rho_{j,M}$ for the bond-distorted lattices; due to the coexistence of the BOW and the CDW, measuring this CDW amplitude that results as a consequence of the external modulation of the hopping integrals is exactly equivalent to the measurement of the bond order differences in the charge-modulated lattices; and (iii) the z-z component of the spin-spin correlations, for a variety of U , V and t_{\perp} . A decreasing ΔE as a function of t_{\perp} signals the destruction of the distortion by increasing two-dimensionality, while a constant or increasing ΔE indicates a persistent distortion^{1,3}. Similarly, decreasing charge ordering for *fixed* bond distortion, as a function of t_{\perp} , indicates also

the tendency to decreasing bond distortion (since the BOW and the CDW are coupled cooperatively), while constant or increasing charge ordering indicates persistent bond distortion.

The modulations of the hopping integrals are determined by

$$\begin{aligned} u_{j,M} &= u_0[(-1)^M r_{2k_F} \cos(2k_F j a - \pi/4) \\ &\quad + r_{4k_F} \cos(4k_F j a)] \\ &= u_0[(-1)^M r_{2k_F} \cos(\pi j/2 - \pi/4) \\ &\quad + r_{4k_F} \cos(\pi j)] \end{aligned} \quad (12)$$

where r_{2k_F} and r_{4k_F} are the amplitudes of the $2k_F$ and $4k_F$ distortions of $u_{j,M}$, respectively. As usual, the index “ j ” labels the sites along a given chain, while “ M ” labels the different chains. Hence the bonds are distorted only along the chains. Our many-body calculations show that this choice of distortions leads the following density waves:

(1) an intrachain CDW,

$$\begin{aligned} \rho_c(j) &\equiv \left\langle \sum_{\sigma} c_{j,M,\sigma}^{\dagger} c_{j,M,\sigma} \right\rangle \\ &= 0.5 + \rho_0 \cos(2k_F j a - 3\pi/4) \\ &= 0.5 + \rho_0 \cos(\pi j/2 - 3\pi/4); \end{aligned} \quad (13)$$

(2) an intrachain SDW,

$$\begin{aligned} \rho_s(j) &\equiv \left\langle c_{j,M,\uparrow}^{\dagger} c_{j,M,\uparrow} - c_{j,M,\downarrow}^{\dagger} c_{j,M,\downarrow} \right\rangle \\ &= \rho_{s2k_F} \cos(2k_F j a - \pi/4) + \rho_{s4k_F} \cos(4k_F j a - \pi) \\ &= \rho_{s2k_F} \cos(\pi j/2 - \pi/4) + \rho_{s4k_F} \cos(\pi j - \pi); \end{aligned} \quad (14)$$

and (3) an intrachain BOW,

$$\begin{aligned} \left\langle \sum_{\sigma} B_{j,j+1,M,M,\sigma} \right\rangle &= b_0 + b_{2k_F} \cos(2k_F j a - \pi/2) \\ &\quad + b_{4k_F} \cos(4k_F j a - \pi) \\ &= b_0 + b_{2k_F} \cos(\pi j/2 - \pi/2) \\ &\quad + b_{4k_F} \cos(\pi j - \pi), \end{aligned} \quad (15)$$

where the phase angles of the DW’s given correspond to odd M , and their amplitudes depend on U, V , and t_{\perp} . As discussed in Section III, we expect (and have verified) the existence of a π phase shift between adjacent chains.

In order to determine the correct behavior in the thermodynamic limit from finite-size simulations, we choose lattices and boundary conditions based on the physical requirement that *for noninteracting electrons any nonzero t_{\perp} must destabilize the BCDW on that particular finite lattice*. This condition simulates the absence of nesting for nonzero t_{\perp} . Our choice of boundary conditions is discussed below. For the monatomic 1/4-filled lattice we have studied both $r_{4k_F} = 0$ and $r_{4k_F} = r_{2k_F}$, establishing that while the magnitude of ΔE does depend on the ratio r_{4k_F}/r_{2k_F} , its behavior as a function of t_{\perp} does not, provided only that $r_{2k_F} \neq 0$; this result is not surprising, since the same CDW coexists with

both BOWs²⁷. We present here detailed results for the case $r_4 = 0$ primarily because for $r_4 \neq 0$, one-electron band-structure effects preclude equally detailed CPMC calculations for the largest lattices. We have, however, pointed out in the above the similarity between $r_4 \neq 0$ and the dimerized dimer lattice, for which the band-structure related effects are less severe, so that we are able to perform our calculations for all the lattices. Note also that the magnitudes of ΔE for the noninteracting and the interacting cases are very different: Coulomb interactions reduce the $\Delta E_0 \equiv \Delta E|_{t_{\perp}=0}$ considerably. However, this merely indicates that for a given e-ph interaction the magnitude of the distortion is less for correlated electrons than for noninteracting electrons. Since, however, the interacting single chain *is* distorted^{16–19,27}, and since our interest lies solely in determining the behavior as a function of t_{\perp} , the relevant quantity is not the absolute value of ΔE but the *normalized* energy gained per site upon distortion, *i.e.*, $\Delta E/\Delta E_0$ for given U and V . This argument is similar to that made by Anderson³³ for perturbative treatments of coupled chains, *viz.*, the sequence in which the intra-chain Coulomb interactions and inter-chain hopping are included is important, and a correct physical picture is obtained only by first including the Coulomb interactions.

A. Methods

The CPMC ground-state quantum Monte Carlo method⁵⁹ uses a constraining trial wavefunction to eliminate exponential loss of signal due to the Fermion sign problem. The method has been thoroughly benchmarked against known results for a variety of different 2D systems and has been shown to produce quite accurate results. However, since the method is non-variational, it is important to check its accuracy in every new system against exact results and to use a variety of different trial wavefunctions. In particular, none of the previous CPMC benchmarks has tested the accuracy of the method when the V interaction is included. The current application of CPMC is also different in the region of filling being investigated, as all previous applications of CPMC to Hubbard models were near half-filling, in order to simulate holes in a 2D AFM appropriate for the cuprate high temperature superconducting materials. At 1/4-filling, the sign problem is typically not as severe as at is for the moderately doped 1/2-filled band, although including the extended interaction lessens this advantage. One of the most important factors to consider in obtaining accurate results with the CPMC method is whether the non-interacting system and trial wavefunctions are degenerate *i.e.* “closed shell” configurations have significantly smaller systematic error in the CPMC approach. As explained in the next section, the appropriate boundary conditions require degeneracy in the non-interacting system for $t_{\perp} \rightarrow 0$. Thus we may expect some prob-

lens with the constrained path approximation for lattices close to $t_{\perp} = 0$. In addition, the isotropic limit $t_{\perp} \rightarrow t$ introduces other degeneracies that cause problems for $t_{\perp} \sim t$. We have checked the accuracy of the method in detail for the 8×2 lattice.

Fig. 4 summarizes the results of the bench-mark calculations for an 8×2 lattice, periodic in the x-direction, with $U = 6$ and $V = 1$. Both undistorted and and the $2k_F$ ($r_{2k_F} \neq 0, r_{4k_F} = 0$) bond distorted systems were compared. For the uniform lattice all hopping integrals taken to be -1.0 , while for the distorted system they were $-1.14, -1.0, -0.86$ and -1.0 . For this amplitude of the $2k_F$ distortion, the absolute value of ΔE is only 0.3% of the total energy (at $t_{\perp} = 0.4$). Such a small energy difference is not easy to measure within QMC. However, for the $2k_F+4k_F$ and dimerized dimer lattice distortions, ΔE is larger, $\sim 0.5\%$. We note that energy differences of this order of magnitude have also been calculated

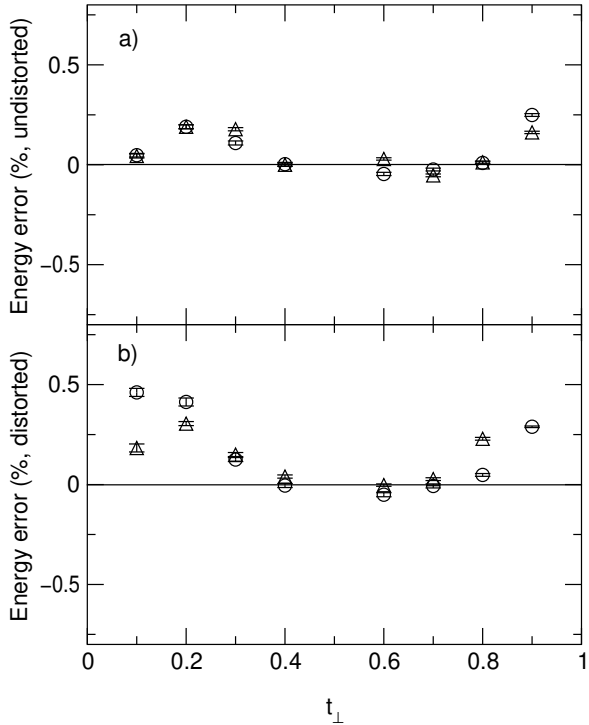


FIG. 4. Percent errors in the CPMC energies for (a) undistorted and (b) $2k_F$ bond-distorted (the hopping integrals in the distorted lattice correspond to those in Fig. 2(a)) 8×2 lattices with $U = 6$ and $V = 1$. Triangles are for the free-electron trial function; circles for the UHF trial function.

using CPMC to study hole binding in the the 3-band Hubbard model⁶⁰. The CPMC values are scaled for $\Delta\tau \rightarrow 0$ from $\Delta\tau = 0.05$ and $\Delta\tau = 0.1$ to remove the Trotter discretization error. The trial wavefunctions used were either the free-electron wavefunction, or an Unrestricted Hartree-Fock (UHF) wavefunction with $U = 2$ and $V = 0.5$. Hartree-Fock wavefunctions with larger U and V gave less accurate results, probably due to the ten-

dency of UHF to exaggerate AFM correlations. In Fig. 4 the UHF trial functions produced larger errors than the free-electron trial functions for the distorted system at small t_{\perp} because the SDW correlations there are exaggerated by the UHF approximation. The CPMC systematic errors are largest at small ($t_{\perp} < 0.2$) and large ($t_{\perp} > 0.8$) possibly due to the degeneracies in the one-electron occupancies at $t_{\perp} = 0$ and $t_{\perp} = t$. However, at large t_{\perp} , the UHF trial wavefunction produced slightly more accurate results for the 8×2 distorted lattice possibly because the numerically-derived UHF wavefunction breaks some of the symmetry of the non-interacting wavefunction. In the intermediate $t_{\perp} \sim 0.4$ regime, the CPMC energies are indistinguishable from the exact energies within the statistical error. The accuracy of the CPMC method in this region is very reassuring, since for the *noninteracting* case, at $t_{\perp} = 0.4$ the distortion has already vanished.

j	$\langle \rho_j \rangle$		$\langle s_i^z s_j^z \rangle$		
	exact	CPMC	i,j	exact	CPMC
1	0.4799	0.4756(6)	1,9	-0.06095	-0.0585(7)
2	0.5201	0.5250(6)	1,10	-0.03215	-0.0312(7)
3	0.5201	0.5240(6)	1,11	0.01408	0.0161(7)
4	0.4799	0.4772(6)	1,12	-0.02698	-0.0231(6)
			1,13	-0.07299	-0.0687(6)
			1,14	-0.03085	-0.0268(5)
			1,15	0.01408	0.0158(6)
			1,16	-0.02552	-0.0239(7)

Table I. Comparison of CPMC and exact charge density and spin-spin correlations for an 8×2 system with $U = 6$, $V = 1$, $t_{\perp}=0.4$, with the same distortion of hopping integrals as in Figure (4). Sites on the first chain are numbered 1 – 8, those on the second chain 9 – 16.

In addition to comparing energies, Table I compares the charge densities and spin-spin correlations computed by CPMC for the 8×2 distorted lattice at $t_{\perp} = 0.4$. The agreement with the exact result is not as good as for the energy (typically 1-5% for the charges and 5-10% for the spin-spin correlations), but is more than adequate to identify the presence and periodicity of the broken symmetry states. Thus in general, we find the CPMC results are close to the exact results for both energies and correlation functions, except for very small or large t_{\perp} .

B. Boundary Conditions

As noted above, we determine the proper combinations of lattices and boundary conditions for the numerical simulations by the requirement that nonzero t_{\perp} destabilizes the BCDW for *noninteracting* electrons with those boundary conditions on that particular finite lattice: *i.e.*, we require the finite lattices to reflect correctly the known behavior of the noninteracting case in the thermodynamic limit.

Consider an $N \times M$ lattice, with N sites along the chain and M chains. To avoid odd/even effects, consider an even number of electrons per chain. This number can then be either $4n$ or $4n + 2$, where n is an integer. To obtain a 1/4-filled band, one can then have $N = 4n \times 2 = 8n$ or $N = (4n + 2) \times 2 = 8n + 4$. The proper N for our purpose is $N = 8n$ (*i.e.*, $4n$ electrons per chain). This follows from the one-electron energy levels of coupled chains with $4n$ and $4n + 2$ electrons per chain. In Fig. 5 below we have shown the one-electron energy levels for the undistorted 8×2 (top panel, labeled a)) and 12×2 (bottom panel, labeled b)) lattices (both periodic in the x -direction), corresponding to $t_{\perp} = 0$ on the left and 0.1 on the right in both cases. In the 8×2 lattice, the degeneracy at $t_{\perp} = 0$ will lead to spontaneous distortion. For nonzero t_{\perp} and a π -phase shift between chains (which gives lower energy than phase shifts of 0 or $\frac{\pi}{2}$), the pairs of one-electron levels that are coupled by phonons with wave-vector $(2k_F, \pi)$ are $(-\frac{2\pi}{8}, 0)$ and $(+\frac{2\pi}{8}, \pi)$; and $(+\frac{2\pi}{8}, 0)$ and $(-\frac{2\pi}{8}, \pi)$. The finite gap that occurs for $t_{\perp} \neq 0$ between each pair of one-electron levels coupled by the $(2k_F, \pi)$ phonon indicates absence of nesting and the destabilization of the distortion. This energy gap increases with t_{\perp} , leading to a decrease in ΔE with t_{\perp} for $N = 8n$ (see Fig. 6(a) for details), as occurs in the thermodynamic limit. In contrast, consider the 12×2 lattice, in which the one-electron ground state is non-degenerate. There is now a nonzero energy gap between the levels coupled by the $2k_F$ electron-phonon interaction already at $t_{\perp} = 0$ ($k_x = -\frac{2\pi}{12}$ and $k_x = +\frac{4\pi}{12}$; $k_x = +\frac{2\pi}{12}$ and $k_x = -\frac{4\pi}{12}$). With nonzero t_{\perp} , and once again a π -phase shift between the chains,

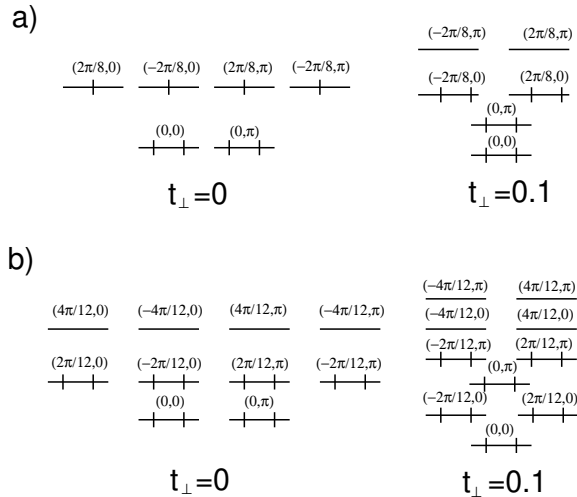


FIG. 5. Occupancies of the one-electron levels for the undistorted (a) 8×2 lattice, with $t_{\perp} = 0$ (left) and $t_{\perp} = 0.1$ (right) and (b) 12×2 lattice, also with $t_{\perp} = 0$ (left) and $t_{\perp} = 0.1$ (right).

the energy gap between the levels $(-\frac{2\pi}{12}, \pi)$ and $(+\frac{4\pi}{12}, 0)$, and similarly that between the levels $(+\frac{2\pi}{12}, \pi)$ and $(-\frac{4\pi}{12}, 0)$, *decreases*, indicating that the tendency to

distort here *increases with inter-chain coupling*, at least for small to moderate t_{\perp} .

For large N , the difference between $N = 8n$ and $N = 8n+4$ vanishes, as is shown in Fig. 6, where Figs. 6(a) and (b) show the behavior of $\Delta E(t_{\perp})$ for $N = 8n$ and $8n+4$, respectively. The qualitative behavior (destabilization of the distortion) is the same for all $N = 8n$, and monotonically decreasing ΔE is also seen for $N = 8n+4$ for large N , but finite size effects (increasing ΔE at small to intermediate t_{\perp}) are strong even for $N = 28$, a chain length already too large for accurate 2D many-body calculations. The correct qualitative behavior of all $N = 8n$ is the basis of our choice of these N .

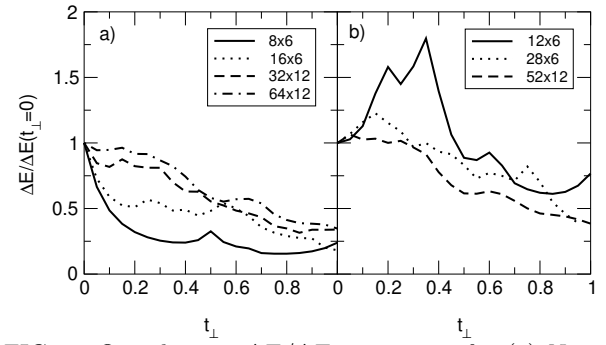


FIG. 6. One-electron $\Delta E/\Delta E_0$ versus t_{\perp} for (a) $N = 8n$ and (b) $N = 8n+4$. In each case results for several $N \times M$ lattices are shown.

In contrast to the choice of N , there is no immediate restriction on the choice of M , the number of chains, except that M should be even, to avoid even/odd effects. $M = 4n$ and $4n + 2$ both show the same qualitative behavior, as seen from the plots of ΔE versus t_{\perp} in Fig. 7, for several $M = 4n$ lattices ($M = 4n + 2$ are included in Fig. 6). Thus both $M = 4n$ and $4n + 2$ are appropriate. Our choice of $M = 4n + 2$ is based on two reasons. First, exact diagonalization calculations on the 8×2 lattice allows comparisons to results obtained within CPMC, and the exact diagonalizations cannot be done for the next larger appropriate lattice, *viz.* 8×4 . Second, the $M = 4n$ lattices are characterized by one-electron Fermi level degeneracies for $t_{\perp} \neq 0$ (even though the degenerate levels are not coupled by $(2k_F, \pi)$ phonons), and the absence of a single well-defined one-electron wave-function would make the CPMC calculations considerably more difficult than for $M = 4n + 2$ lattices, which have non-degenerate one-electron levels for nonzero t_{\perp} .

The restriction to $N = 8n$ sites coupled with the 1/4-filling introduces a potential subtlety into the numerical computations of $\Delta E/\Delta E_0$ for nonzero U and V . Finite 4n-electron 1D undistorted periodic rings have their ground state in the total spin $S = 1$ subspace, and even the distorted system's ground state can be in the $S = 1$ subspace for the smallest 4n-electron rings. We have confirmed from exact diagonalizations of the 8×2 lattice that the ground state is in the $S = 0$ state for the smallest

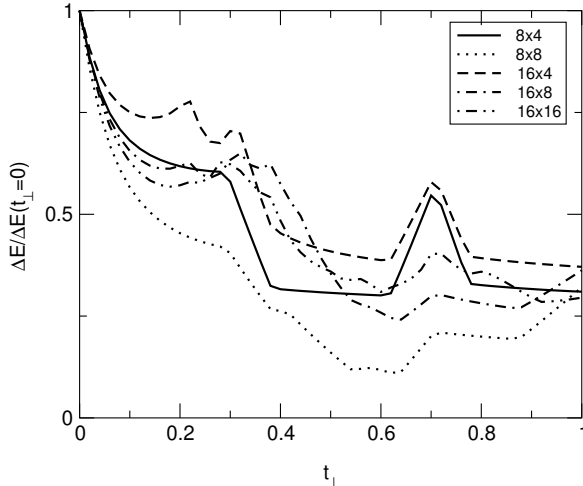


FIG. 7. One-electron $\Delta E/\Delta E_0$ for the 8×4 , 8×8 , 16×4 , 16×8 and 16×16 lattices for the $2k_F$ bond distortions as in Fig. 2(a).

nonzero t_\perp , as might be anticipated from Fig. 5. Thus while ΔE_0 can correspond to the energy gained upon distortion in the $S = 1$ subspace, ΔE necessarily corresponds to the energy gained upon distortion in the $S = 0$ subspace. As this important but subtle point requires extensive discussion that would interrupt the presentation here, we present the details in the Appendix, where we show that despite this subtlety, the behavior of $\Delta E/\Delta E_0$ nevertheless is a proper measure of the stability of the distorted state for nonzero t_\perp .

C. UHF calculations

In this section we discuss mean-field UHF results for Hamiltonian (1). Although the UHF wavefunction is typically a poor approximation to the ground state for strongly-correlated systems, one reason for performing these calculations is to have another single-determinant trial wave function (apart from the non-interacting case) available for CPMC simulations. Furthermore, much larger systems can be simulated than with CPMC.

Our numerical UHF method solves the UHF self-consistent equation on finite-size lattices. We have chosen relatively small U and V for two reasons: the UHF procedure does not converge well for larger interactions, and the smaller values of U and V gave better results when used as a CPMC trial function (compared to a numerically exactly solved 8×2 system). Fig. 8 shows the normalized energy gain from a $2k_F$ distortion for two different lattices, within the UHF approximation. The UHF results show that $\Delta E/\Delta E_0$ remains close to 1 for at least up to $t_\perp \sim 0.4$, indicating a tendency to persistent distortion up to this t_\perp . Although $\Delta E/\Delta E_0$ begins to decrease at still larger t_\perp , these calculations are for a relatively small value of U , and as discussed in section III, the range of t_\perp over which the distortion should persist increases with U . Thus the qualitative effects of the

e-e interaction are already visible within the UHF approach at small U , while a fully persistent broken symmetry state will occur only for larger values of the e-e interaction that are beyond the scope of the UHF.

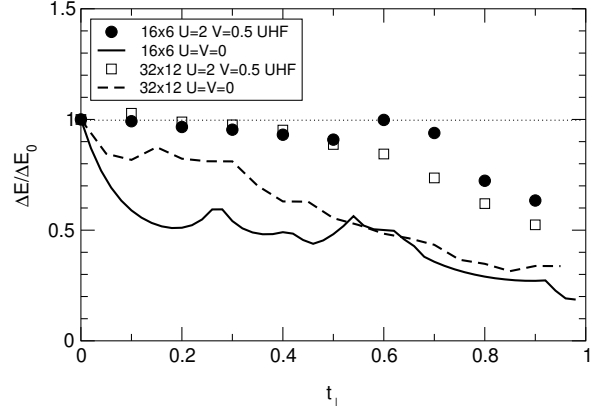


FIG. 8. $\Delta E/\Delta E_0$ versus t_\perp for a $2k_F$ bond distortion ($r_{4k_F} = 0$) for noninteracting and the interacting lattices within the UHF approximation. Intra-chain hopping integrals for the distorted lattices are as indicated in Fig. 2(a).

Given that the UHF approximation predicts a vanishing of the bond dimerization in the $1/2$ -filled band for a fairly small U_c (the actual magnitude of U_c depends on α), in contrast to the correct result that there is an enhancement of the dimerization¹ for $0 < U < 4$, the present results, showing a persistence of the distortion for moderate t_\perp , is initially perplexing. Further consideration shows that the reason for the correct prediction (see below for the numerical results) in this case is that the UHF exaggerates the SDW, which destroys the BOW in the $1/2$ -filled band, but has a co-operative interaction with the $1/4$ -filled band for small to moderate t_\perp .

D. Exact diagonalization and CPMC calculations, $r_{4k_F} = 0$

In Fig. 9 we show the behavior of $\Delta E/\Delta E_0$ for the non-interacting and interacting ($U = 6, V = 1$) cases for three different lattices satisfying our boundary condition constraints. In all cases we measure the electronic energy gained upon $2k_F$ SUWU bond distortion (corresponding to nearest neighbor hopping integrals $t_S = -1.14$, $t_U = -1.0$, and $t_W = -0.86$), relative to that of the undistorted state with equal hopping integrals. For the 8×2 lattice the calculations involved both exact diagonalization and the CPMC technique. The 8×2 results, taken together, then provide an estimate of the precision of the CPMC calculation. The exact diagonalization studies also confirmed that the system is in the total spin state $S = 0$ for t_\perp as small as 0.01 (see Appendix).

The large scatter in the normalized ΔE at very large and very small t_\perp may be due to the degeneracies in the non-interacting system at $t_\perp \rightarrow 0$ and $t_\perp \rightarrow 1$.

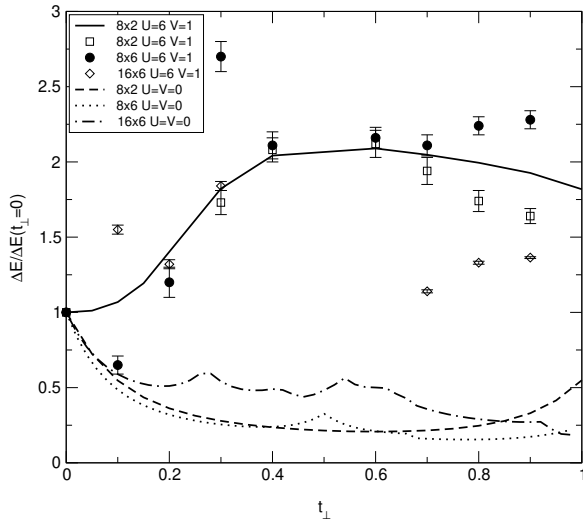


FIG. 9. $\Delta E/\Delta E_0$ versus t_\perp for a $2k_F$ bond distortion ($r_{4k_F} = 0$) for the 8×2 , 8×6 , and 16×6 lattices for $U = V = 0$ and for $U = 6$, $V = 1$. For the 8×2 lattice both exact (solid line) and CPMC results are shown. Intrachain hopping integrals for the distorted lattices are as indicated in Fig. 2(a).

Furthermore, as mentioned in the methods section above, the absolute values of ΔE are rather small, especially for the pure $2k_F$ ($r_{4k_F} = 0$) distortion. The systematic errors due to the CPMC approximation are therefore large in these two regions. Nevertheless, except for the $\Delta E/\Delta E_0$ value at $t_\perp = 0.1$ for the 8×6 lattice, at all other t_\perp the $\Delta E/\Delta E_0$ values are above 1 for all three lattices, and far above the normalized non-interacting values. As seen in Fig. 9, while for the non-interacting cases the $\Delta E/\Delta E_0$ decreases rapidly with t_\perp , for the interacting cases the $\Delta E/\Delta E_0$ either remains unchanged or is enhanced by t_\perp . Because of the strong degeneracies in the one-electron occupancy scheme at the Fermi level at $t_\perp = 1$, a single well-defined one-electron wavefunction is missing here. The CPMC calculations therefore could not be done for $t_\perp = 1.0$. It is, however, highly unlikely that the BCDW persists for $t_\perp = 0.9$ but vanishes at $t_\perp = 1$; this expectation is corroborated by the results of the exact diagonalization studies for the 8×2 lattice, which were performed for the full range of t_\perp , including $t_\perp = 1$ and showed enhanced distortion throughout the whole region. In the following sections we also show $\Delta E/\Delta E_0$ for the $2k_F+4k_F$ ($r_{4k_F} \neq 0$) and dimerized dimer lattice. In both of these cases, the magnitude of ΔE is larger and hence easy to compute, but degeneracies restrict CPMC simulations to smaller t_\perp . In both cases, $\Delta E/\Delta E_0$ is close to or above 1 for all t_\perp we have studied.

As discussed in the above, the bond-distorted lattices (both $r_{4k_F} = 0$ and $r_{4k_F} \neq 0$) have a synergetic coexistence with the CDW. Thus the amplitude of the CDW, defined as $\Delta\rho_c = \rho_{cl} - \rho_{cs}$, where ρ_{cl} and ρ_{cs} are the larger and smaller charge densities on the ...1100... $2k_F$ CDW, is an alternate measure of the stability of the BOW. If the

nonzero t_\perp destabilized the bond-distortion, then even with *fixed* $2k_F$ distorted hopping integrals the amplitude of the BOW (measured as the differences in the bond orders) would decrease, and the diminished strength of the BOW in turn would decrease $\Delta\rho_c$. This is easily confirmed for the noninteracting Hamiltonian, where the amplitude of the CDW decreases with increasing t_\perp . In Fig. 10(a) we show the charge densities on a single chain for a bond-distorted 8×6 lattice (because of periodicity, all chains are equivalent) for $U = 6$, $V = 1$, and $t_\perp = 0.2$. In Fig. 10(b) we have shown the behavior of $\Delta\rho_c$ for all the three lattices we have studied, now as a function of t_\perp . Degeneracies in the one-electron energy levels in the 16×6 lattice for $t_\perp > 0.6$ even with finite bond-distortion cause the CPMC ground states in this region to be $S = 1$. Exact calculations in the 1D limit show that the amplitude of the CDW in $S = 1$ is less than that in $S = 0$. Thus the weak decrease in the $\Delta\rho_c$ values with t_\perp in the 16×6 lattice is a spin effect: the bond distorted state is $S = 0$ at small t_\perp and $S = 1$ at large t_\perp . The $\Delta\rho_c$ values at large t_\perp for the 16×6 lattice should therefore be considered as *lower limits* (the $\Delta\rho_c$ values of the 16×6 lattice are considerably larger than that of the $S = 1$ single chain of 16 sites).

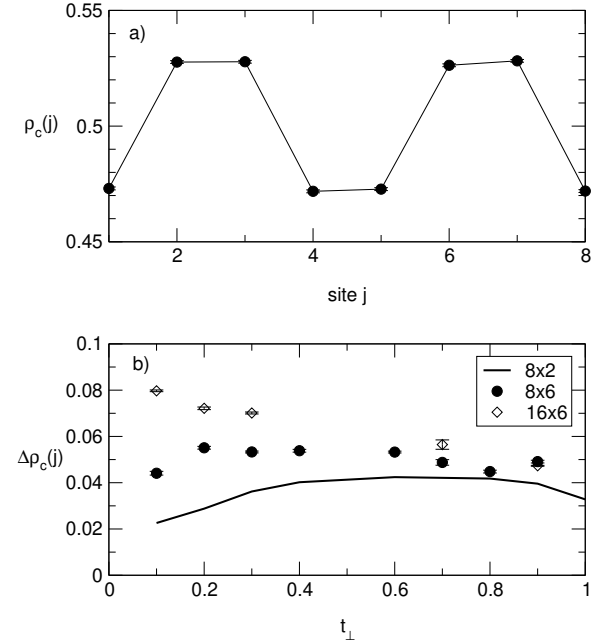


FIG. 10. (a): Site charge densities on one of the 6 chains in a $2k_F$ bond-distorted 8×6 lattice, for $t_\perp = 0.2$, $U = 6$, and $V = 1$. The line is meant as a guide to the eye. Note the expected "...1100.." structure discussed in the text. (b) Amplitude of the $2k_F$ CDW for the $2k_F$ bond-distorted 8×2 (exact), 8×6 , and 16×6 lattices. The ground state of the 16×6 lattice is in the $S = 1$ subspace for $t_\perp > 0.6$, and the CDW amplitudes for the $S = 0$ states here are expected to be greater than those calculated for the ground state and shown in the Fig. (see text).

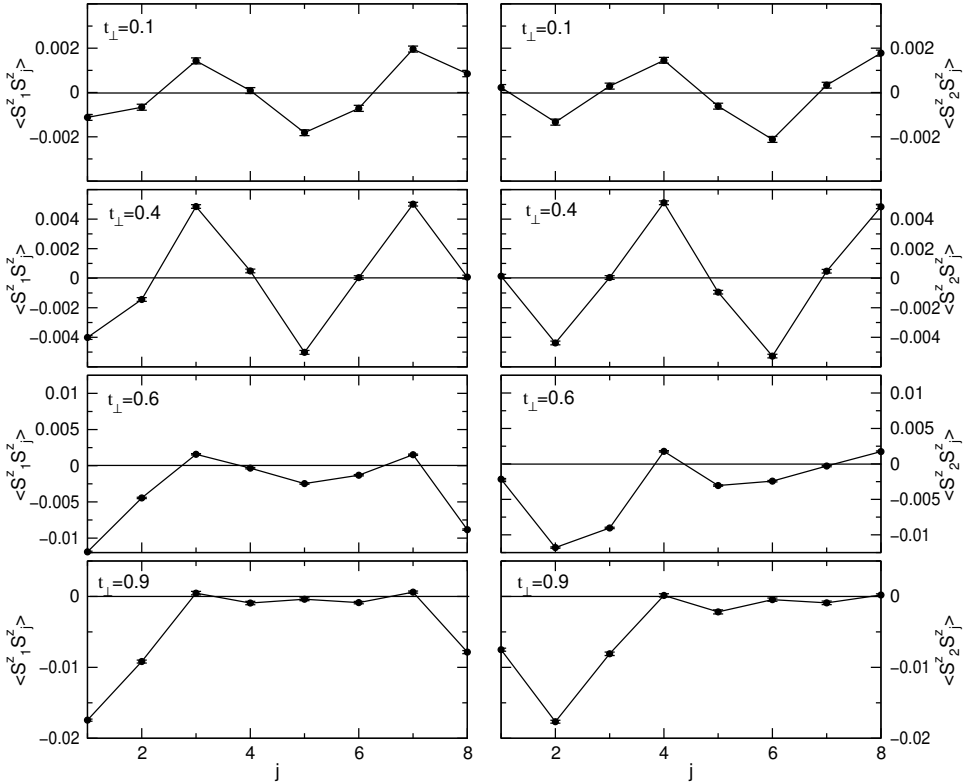


FIG. 11. The z-z spin correlations between sites 1 (left panels) and 2 (right panels) on the first chain of the 8×6 lattice and sites $j = 1 - 8$ on the second chain, with $U = 6$, $V = 1$ for four values of t_{\perp} . Due to finite size effects the wavefunction has small admixing with the ...1010... charge order which affects the individual magnitudes of the spin-spin correlations (see text). AFM correlations increase with t_{\perp} up to $t_{\perp} = 0.4$ but then vanish at $t_{\perp} \simeq 0.6$, even though the BCDW continues to persist for all t_{\perp} (see Fig. 10). Lines are guides to the eye.

In agreement with the behavior of the ΔE in the interacting case (see Fig. 9), the CDW amplitude now *increases* or remains constant with increasing t_{\perp} for all the lattices studied, indicating a greater tendency to bond and charge distortion with increasing t_{\perp} . *Taken together, the results of Figs. 9 and 10 provide quantitative proof of our qualitative arguments establishing that the BCDW is a robust broken symmetry state for the interacting 2D $\frac{1}{4}$ -filled band.*

In Fig. 11 we show the inter-chain spin-spin correlations between sites 1 and 2 on the first chain, and sites $j = 1 - 8$ on the second chain, for the $2k_F$ bond-distorted 8×6 lattice for several values of t_{\perp} . The SDW profile is somewhat different from what is expected from a pure ...1100... charge modulation along the chains because the wavefunction of this finite lattice also has contributions from the ...1010... type intrachain charge modulation. The small ...1010... contribution to the wavefunction affects the charge density, $n_{j,M,\uparrow} + n_{j,M,\downarrow}$ only weakly, but the spin density, being the difference $n_{j,M,\uparrow} - n_{j,M,\downarrow}$ is a smaller quantity and is affected relatively more strongly. It is useful here to recall however that within the rectangular lattice, ...1010... charge orderings along both longitudinal and transverse directions give triangular lattice of occupied sites, and thus a pure ...1010... cannot give the SDW profiles of Fig. 11 (see also below)⁶¹.

Qualitatively, at $t_{\perp} = 0.1$ the SDW behavior is the

same as in Ref. 24, where these calculations were done for the 12×4 lattice: the amplitude of the interchain spin-spin correlation is independent of the distance between the sites, indicating long-range order. The qualitative behavior of the spin-spin correlations is the same for $t_{\perp} = 0.4$, where, however, the amplitude of the SDW is larger. At still larger t_{\perp} ($= 0.6$), the inter-chain correlations are very strongly antiferromagnetic at short distances ($j = 1, 2$ on chain 2), but the antiferromagnetic correlations have disappeared at larger distances. This can be seen from comparisons of the spin-spin correlations corresponding to values of j lying near the center of the second chain ($j = 5$), which are farthest from the spins occupying sites 1 and 2 on the first chain. While the spin-spin correlations near this j increase from $t_{\perp} = 0.1$ to 0.4, they decrease as t_{\perp} is further increased to 0.6. Similarly, focusing on site 8 of the second chain, we see that the spin-spin correlation with site 1 on the first chain has actually changed sign upon increasing t_{\perp} to 0.6 from 0.4 (due to the very strong short-range antiferromagnetic correlations), and the magnitude of the positive spin-spin correlation with site 2 on the first chain has decreased. All of these results indicate the absence of long-range spin order for large $t_{\perp} \geq 0.6$ in the 8×6 lattice. The loss of the long-range spin-order is most clear at $t_{\perp} = 0.9$, where spin-spin correlations are nonzero only for the nearest interchain neighbors.

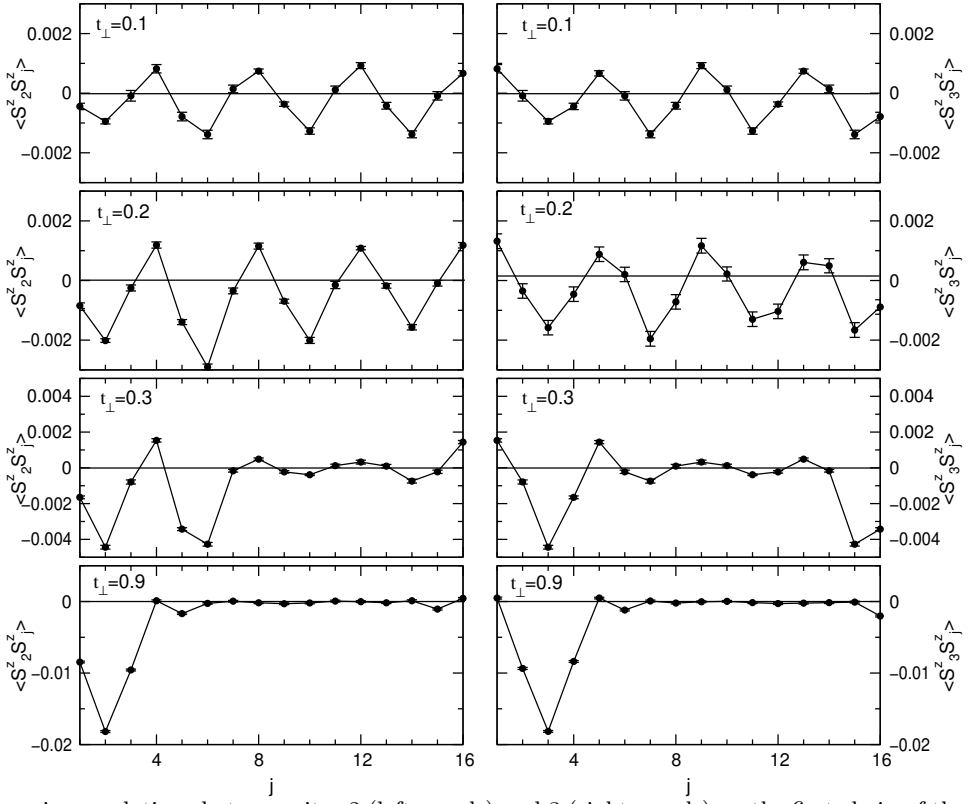


FIG. 12. The z-z spin correlations between sites 2 (left panels) and 3 (right panels) on the first chain of the 16×6 lattice and sites $j = 1 \dots 16$ on the second chain, with $U = 6$, $V = 1$ for four different values of t_{\perp} . The finite size effects, and contamination with the ...1010... charge order here is smaller than in Fig. 11. Lines are guides to the eye.

Fig. 12 shows the inter-chain spin-spin correlations between sites 2 and 3 on the first chain and sites $j = 1 \dots 16$ on the second chain for the 16×6 lattice. The admixture of the intrachain ...1010... CDW is weaker in this larger system (this is because the “tunneling” between the extreme configurations ...1100... and, say, ...0110..., decreases with size, and as consequence, V_c increases with size in finite systems). This can be seen by simply comparing the figures on the left and right panels for $t_{\perp} = 0.1$ and 0.2. If the intrachain CDW were a pure ...1010..., the signs of the spin-spin correlations for each j would be the same for both $i = 2$ and $i = 3$. Different signs for these correlations are signatures of the ...1100... CDW (see Fig. 2). As in the 8×6 system, long-range SDW behavior is seen for $t_{\perp} = 0.1$. Focusing on sites $j = 7 \dots 12$ on the second chain, the amplitude of the SDW increases from $t_{\perp} = 0.1$ to $t_{\perp} = 0.2$, but further increasing t_{\perp} to 0.3 destroys the long-range order, as evidenced again by very large AFM correlations at short distances and vanishing correlations at large distances (sites $j = 7 \dots 12$ on the second chain). The vanishing of the SDW is seen most clearly at very large t_{\perp} ($t_{\perp} = 0.9$ in Fig. 12) a region where calculations of ΔE and charge densities still show a persistent BCDW. We observe this same behavior of the SDW on 8×2 lattice. In all cases, the SDW amplitude initially increases, exhibits a maximum, and then vanishes at a t_{\perp}^c which decreases with the size of the system. As discussed in section III.D, this behavior is to be

expected from the nature of the BCSDW in Fig. 2. The initial increase of the SDW amplitude indicates that t_{\perp}^c is nonzero, a conclusion that is also in agreement with the experimental observation of the BCSDW state in the weakly 2D organic CTS (see below). Based on the calculations for 16×6 lattice, we estimate $0.1 < t_{\perp}^c < 0.3$ for the strictly rectangular lattice for $U = 6$, $V = 1$.

E. Persistent distortions with $r_{4k_F} \neq 0$

The bond modulation pattern in the 1/4-filled band given in Eq. (7) has in general both $2k_F$ and $4k_F$ components. Figs. 9 and 10 show persistent distortion at large inter-chain couplings for $r_{4k_F} = 0$ (purely $2k_F$ bond distortion). The persistent BCDW is expected also for $r_{4k_F} \neq 0$. Physically, the reason for this persistence is the *coexisting* site CDW, whose nature is independent of r_{4k_F} ^{24,27}. We show in Fig. 13 the calculated $\Delta E/\Delta E_0$ for $r_{4k_F} = r_{2k_F}$ (equal admixtures of $2k_F$ and $4k_F$ bond distortions), for the 8×2 and 8×6 lattices for $U = 6$ and $V = 1$. The hopping integrals corresponding to the distorted lattice here are -1.089 , -0.974 , -1.089 and -0.848 , and the energy gained is being measured against the uniform lattice. Starting from $t_{\perp} = 0.5$, the one-electron ΔE is highly discontinuous. This is because distortion with $r_{4k_F} \neq 0$ does not correspond to a natural periodicity for the noninteracting system. As a consequence the

noninteracting wavefunctions are not suitable trial wavefunctions for the CPMC calculation. For the same reason the 16×6 calculation could not be performed here. The similarities between the results for the 8×2 and the 8×6 lattices are obvious. The ratio $\Delta E/\Delta E_0$ is independent of t_\perp over a broad range of t_\perp , and increases slightly for large t_\perp , indicating once again a stable 2D BCDW. Although only limited data could be obtained for this case, the dimerized dimer lattice is very similar in character to $r_{4k_F} \neq 0$ (see Fig. 2(b)). In the following we show convincing evidence for persistent double-dimerization in 2D.

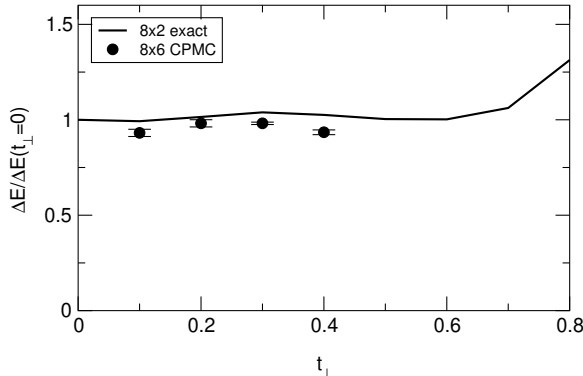


FIG. 13. $\Delta E/\Delta E_0$ versus t_\perp for $r_{4k_F} = r_{2k_F}$ for the 8×2 and 8×6 lattices for $U = 6$, $V = 1$. Intra-chain hopping integrals for the distorted lattices are as indicated in Fig. 2(b).

F. The dimerized dimer lattice

We have previously noted that Fig. 2(b) suggests that an alternate way to view the BCDW/BCSDW states is as a dimer lattice with additional structure within each of the dimer cells; the dotted box in Fig. 2(b) represents one dimer. Each dimer has one electron, leading to an “effective half-filled” dimer band^{37–40,42}. Bond dimerization in the 1D 1/2-filled band is unconditional for all $U > 2V^{1/3}$, and thus this dimer lattice itself distorts in a period 2 dimerization pattern in 1D. In this section we show the additional result that the (anisotropic) 2D dimer lattice is unconditionally unstable to a second dimerization for all t_\perp .

We choose the hopping integrals between the two sites within the dimer cell to be 1.2 in our calculations. The two inter-dimer hopping integrals for the uniform dimer lattice were taken to be 0.8, while for the distorted (“dimerized”) dimer lattice these were taken to be 0.7 and 0.9, respectively (*i.e.*, the dimerized dimer lattice has hopping integrals 1.2, 0.7, 1.2, 0.9 along each chain). Exact diagonalizations show that a π -phase shift between the chains (*i.e.*, dimer cells lying directly above each other, but a strong inter-dimer bond on one chain facing a weak inter-dimer bond on the next chain) gives the lowest total energy. Again we define ΔE and ΔE_0 as the electronic energies gained per site upon bond dis-

tortion by the 2D and 1D lattices. Fig. 14 shows the $\Delta E/\Delta E_0$ behavior for the 8×2 lattice over the complete range of t_\perp and for the 8×6 and 16×6 lattices for several different t_\perp for $U = 6$ and $V = 1$. The 8×6 and 16×6 lattices, taken together, cover nearly the full range of t_\perp , and the $\Delta E/\Delta E_0$ behavior for these lattices closely follow the curve for the 8×2 lattice. As before, $\Delta E/\Delta E_0$ is significantly greater than 1 for the complete range $0 < t_\perp < 1$, indicating the persistence of the dimerization for the non-interacting case, the dimerization vanishes, as expected.

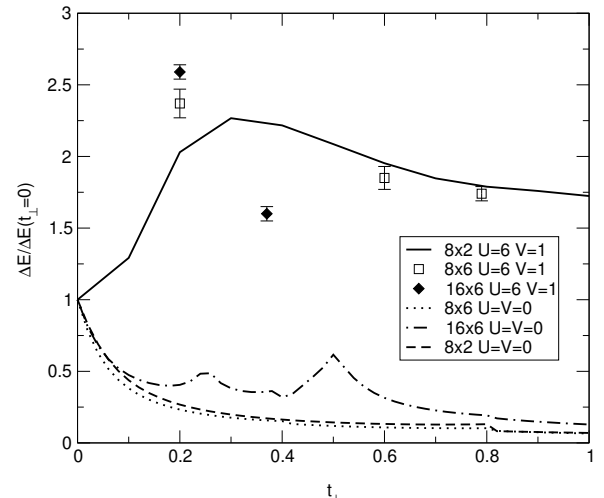


FIG. 14. $\Delta E/\Delta E_0$ versus t_\perp for a dimerized dimer lattice for the 8×2 , 8×6 and 16×6 lattices, for $U = 6$, $V = 1$. The intradimer hopping integrals are 1.2 in both cases. All inter-dimer hopping integrals are 0.8 in the dimer lattice, and 0.7 and 0.9 in the dimerized dimer lattice.

Fig. 15 shows the interchain spin-spin correlations between sites 2 and 3 on one chain and sites $j = 1 - 16$ on a neighboring chain, for a 16×6 dimerized dimer system. Notice the far smaller contribution by the ...1010... intrachain charge ordering here. This is because of the large difference between the hopping integrals even in the “uniform” lattice with interdimer hopping integrals of 0.8 here. Such a large bond dimerization diminishes the intrachain ...1010... contribution. The spin-spin correlation amplitudes cannot be directly compared to Fig. 12 because of the different distortion amplitudes, but Fig. 15 shows that the SDW amplitude is significantly greater in the intermediate t_\perp regime ($t_\perp = 0.37$ in the Figure) compared to the small t_\perp regime unlike the results in Fig. 12. Our calculations indicate that the larger the difference between the intra-dimer and the inter-dimer hopping integrals, the greater the range of the t_\perp over which the SDW is stable. Thus with hopping integrals of 1.2, 0.9, 1.2 and 0.7 along each chain, the SDW in the 8×6 lattice persists even at $t_\perp = 0.6$ (in contrast to the $2k_F$ bond-distorted lattice of Fig. 2), but vanishes at still larger t_\perp . This is expected from our discussion of

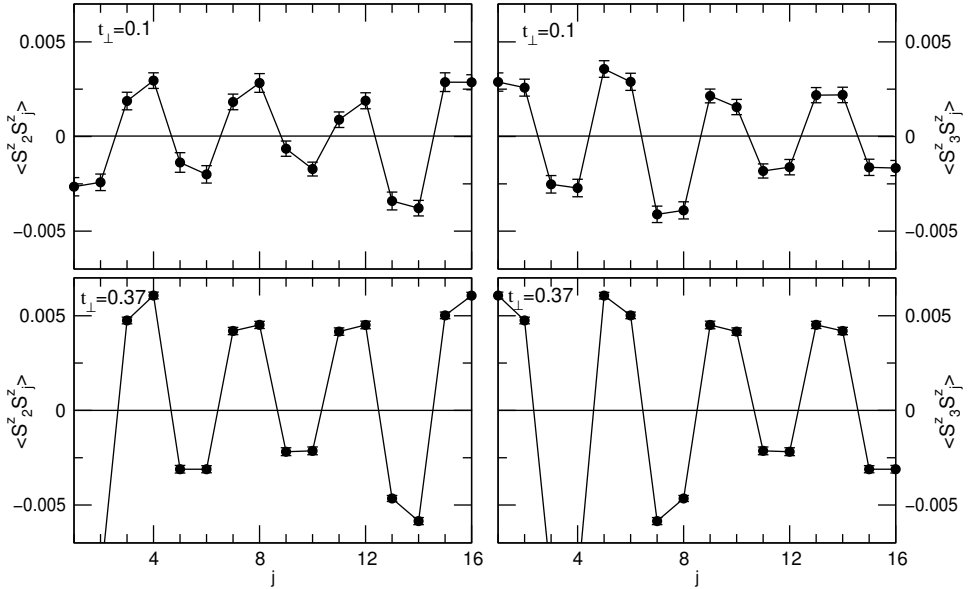


FIG. 15. The z-z spin correlations for the 16×6 dimerized dimer lattice. Correlations are shown between site 2 and site 3 on the first chain and sites 1-16 on the second chain with $U = 6$, $V = 1$ for two values of t_{\perp} (0.1 and 0.37). Lines are guides to the eye.

the behavior of the SDW in Section III.D. Recall that the smaller spin densities on the sites labeled ‘0’ are influenced by both the intra-chain nearest neighbor as well as the inter-chain nearest neighbor with opposite spin, and this competition creates a disordering effect. The larger the hopping integral between the ‘0’ and the nearest intrachain ‘1’, the larger the t_{\perp} necessary to create the disordering of the spin, hence the greater stability of the SDW. We shall later argue that this same phenomenon is related to the very large magnetic moments of the κ -(BEDT-TTF) salts.

G. Effects of additional Coulomb interactions

Fig. 2 clearly suggests that inter-chain nearest neighbor Coulomb interaction V_{\perp} stabilizes the BCDW further. We have confirmed this by exact numerical calculations for the 8×2 lattice, as shown in Fig. 16 below,

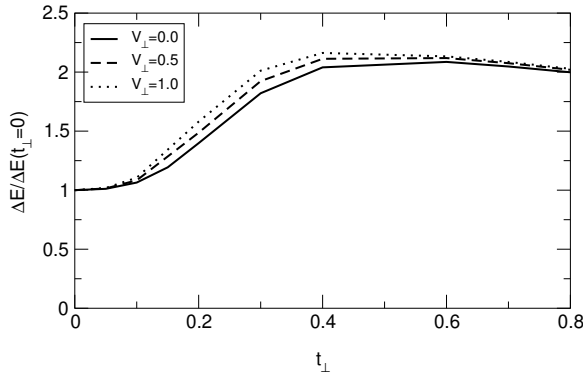


FIG. 16. $\Delta E/\Delta E_0$ vs. t_{\perp} for the 8×2 lattice, with $U = 6$, $V = 1$ and $V_{\perp} = 0, 0.5, 1.0$, for $r_{4k_F} = 0$.

where we have plotted $\Delta E/\Delta E_0$ for three different values of V_{\perp} : 0, 0.5 and 1. Nonzero V_{\perp} increases ΔE further. Similar calculations were done also with variable V_{\perp} but fixed V_{\perp}/t_{\perp} . An even larger increase in ΔE is found in this case. Interchain Coulomb interactions are currently difficult to implement within the CPMC calculations, and therefore these calculations could not be performed for larger lattices. However, based on the similarities between the ΔE behavior of the three lattices studied in Figs. 9 and 14, no difference in the larger lattices is expected.

VI. COMPARISON TO EXPERIMENTS ON THE INSULATING STATES IN 2:1 ORGANIC CTS

Experimentally, the organic cationic CTS, with cation:anion ratio of 2:1, span the range $t_{\perp} \leq 0.1$ in $(\text{TMTTF})_2\text{X}$ to $t_{\perp} \sim 1$ in certain $(\text{BEDT-TTF})_2\text{X}$. Hence these materials provide a critical testing ground for our theoretical results. In reference [24] we compared our theoretical predictions regarding the BCSDW state to the mixed CDW-SDW found experimentally in $(\text{TMTTF})_2\text{Br}$, $(\text{TMTSF})_2\text{PF}_6$ and α -(BEDT-TTF) $_{2-}\text{KHg}(\text{SCN})_4$. Here we make additional, more detailed comparisons, distinguishing between 1D TMTTF and weakly 2D TMTSF-based compounds, and also emphasizing the similarities and differences between the salts of BEDT-TTF and BETS with different crystal structures. Comparisons to the $(\text{TMTTF})_2\text{X}$ and $(\text{TMTSF})_2\text{X}$ are fairly straightforward, as these systems form nearly rectangular lattices. The crystal structures of the BEDT-TTF systems are more complicated and more subtle analyses are required. Our aim is to show that the BCSDW and the BCDW are appropriate de-

scriptions of the insulating states of this entire class of 2:1 cationic CTS, and conversely, the very nature of the insulating ground state in certain cases provides direct verification for some of our more surprising theoretical results. We discuss below each class of material individually.

A. (TMTTF)₂X

The (TMTTF)₂X compounds are nearly 1D semiconducting materials with weak to moderate dimerization along the stacks at high temperature. Because of this dimerization, they have often been described within the effective 1/2-filled band picture^{37,62}. Further dimerization of the dimerization occurs below the SP transition temperature T_{SP} (~ 15 K). Existing theories of the SP transition in these systems⁶² do not discuss the simultaneous appearance of the 2k_F CDW. As depicted in Fig. 1(c), and as confirmed in Fig. 3(d), independent of whether these systems are considered as 1/4-filled or effective 1/2-filled with a dimer lattice, the appearance of this CDW is unconditional. In a recent NMR study of ¹³C spin-labeled (TMTTF)₂PF₆ and (TMTTF)₂AsF₆ charge-ordered states have been found⁶³. Although such a charge-ordering suggests agreement with the theory presented here, one problem is that the initial appearance of the charge-ordered phase occurs considerably above the SP transition temperature T_{SP} ⁶³. There are two possible reasons why the charge-ordering might appear at temperature $T_{CO} > T_{SP}$. First, this might be due to fluctuation effects associated with the 1D nature of the crystals³⁰: at $T < T_{CO}$ the phase relationships between the charge-orderings on individual chains are arbitrary, and only at $T < T_{SP}$ the π -phase shift between nearest neighbors that is necessary for 3D ordering is reached. A second possibility is that the charge-ordering is driven primarily by the Holstein e-ph coupling β in Hamiltonian (1), and the SSH coupling α is small, such that actual lattice displacement and spin singlet formation takes place at lower temperature. Independent of which mechanism dominates to give $T_{CO} > T_{SP}$, it is important to keep in mind that (a) no charge-ordering is expected at all within conventional theories of SP transition, and (b) as discussed extensively in section III, charge ordering of the type ...1010..., as has sometimes been suggested (see below), promotes equal intrachain bonds, and therefore the SP transition cannot occur within such a charge-ordered phase. Finally as has been pointed out by us previously²⁷, charge-ordering of the type ...1100... also occurs in the SP phase of the anionic 1:2 TCNQ solids.

Although most (TMTTF)₂X exhibit the SP transition, the material (TMTTF)₂Br exhibits a transition to a SDW^{64,65}, like the (TMTSF)₂X. Also like the (TMTSF)₂X, this material can become superconducting, although at a relatively high pressure of 26 kbar. Within the structural classification scheme described by

Jerome³², this difference is due to the larger t_{\perp} in (TMTTF)₂Br (relative to the other TMTTF). We therefore discuss this material along with the (TMTSF)₂X.

B. (TMTTF)₂Br and (TMTSF)₂X

X-ray scattering studies by Ravy and Pouget^{36,44} have shown that in both (TMTTF)₂Br and the prototype TMTSF system, (TMTSF)₂PF₆, CDW distortions occur below the SDW transition temperature T_{SDW} . Similar conclusions have been reached also by Kagoshima et al.⁴⁵. In (TMTTF)₂Br evidence for 4k_F lattice instability was found^{36,44}, clearly suggesting that the insulating state here is the BCSDW of Fig. 2(b). In (TMTSF)₂PF₆ the authors claim a “purely electronic CDW”, which would indicate the dominance of the 2k_F CDW over the BOW. Since, however, in both the 1/4-filled band and the effective 1/2-filled band the 2k_F CDW necessarily coexists with a BOW, the experimental work merely indicates that the transition to the BCSDW state is driven mainly by the Holstein e-ph coupling in Eq. (1) rather than the SSH coupling (*i.e.*, α is small), so that the actual modulations of the intermolecular distances are small⁶⁶. This would agree with one of the two possible reasonings given by us for T_{CO} being larger than T_{SP} in (TMTTF)₂PF₆ and (TMTTF)₂AsF₆, as discussed above.

One additional comment appears to be necessary. Fröhlich mode sliding conductivity has been seen in (TMTSF)₂X⁶⁷. While this indicates a weak incommensurability of the density wave (see below), an equally important point is that the sliding conductivity in the past has been ascribed to that of the SDW: the SDW collective transport is viewed as that of two CDWs, one for each spin subband. The actual displacement of the charge density is difficult to visualize in configuration space within this picture. We believe that the experimental demonstration of the coexisting CDW and the present theoretical work, taken together, suggest the more coherent viewpoint that the sliding mode conductivity is that of a BCSDW.

C. α -(BEDT-TTF)₂MHg(SCN)₄

This class of materials, with M = K, Rb, Tl and NH₄ has been of considerable interest recently. M = NH₄ is a superconductor, but M = K, Rb, Tl are non-superconducting. Early magnetic susceptibility studies in the M = K material had indicated anisotropic susceptibility below the so-called “kink” transition that occurs at 10 K, indicating a SDW; here the kink refers to the change in slope that occurs in the temperature dependence of the resistivity and the Hall coefficient. On the other hand, analysis of the angle-dependent magnetoresistance oscillations by Sasaki and Toyota led these authors to conclude already in 1995,

prior to the experiments by Pouget and Ravy in the $(\text{TMTSF})_2\text{PF}_6$, that the dominant broken symmetry in α -(BEDT-TTF)₂MHg(SCN)₄ is a CDW⁶⁸. Since, however, a CDW would not explain the anisotropic susceptibility, Sasaki and Toyota concluded that the broken symmetry here is a “mysterious” state that is a “SDW accompanied by a CDW” or a “CDW accompanied by a SDW”. Muon spin resonance studies indicate very small magnetic moment per BEDT-TTF molecule here, $\sim 0.003 \mu_B$ ⁶⁹ (to be compared against $0.08 \mu_B$ in $(\text{TMTSF})_2\text{X}$ ⁷⁰ and $0.4 - 1 \mu_B$ per BEDT-TTF dimer in κ -(BEDT-TTF)₂Cu(CN)₂Cl⁷¹, see below). More recent ¹³C-NMR studies in the M = Rb indicates even smaller magnetic moment (if it exists at all) $\sim 1 \times 10^{-4} \mu_B$ ⁷². Recent theoretical⁷³ and experimental⁷⁴ investigations conclude either that the dominant broken symmetry here is a CDW or that it is not a conventional SDW⁷⁵.

We point out here that a mixed state with very small magnetic moments is exactly what is expected within our theory. In Fig. 17 we have given a schematic view of the structure of the donor plane in α -(BEDT-TTF)₂MHg(SCN)₄. The one-electron hopping integrals (called “ t_p ” and “ t_c ” in the figure) have been calculated using approximate one-electron techniques by Mori et al.⁷⁶ and Ducasse⁷⁷. Here the t_p correspond to the interstack hopping and the t_c to the intrastack hopping. Four slightly different p-type integrals and three slightly different c-type integrals are obtained by these authors. We ignore the small differences within each type of hopping integrals, as a more important effect is the periodic modulation that appears with the BCDW. We believe that what is relevant in the present context is that $t_p > t_c$. If as a first approximation we therefore ignore the t_c hopping integrals, the lattice is simply a rotated (by approximately 45°) version of our rectangular lattice near $t_\perp \sim 1$. Restoring the c-integrals now gives the same rotated rectangular lattice with one of the two diagonal hopping integrals t_{diag} as nonzero. Our calculations (see Figs 9 – 15) show that even at $t_\perp \sim 1$ the correlated 1/4-filled band (or the dimerized dimer lattice) remains bond and charge-distorted, while based on the ...1100... ordering along the diagonals we have argued that t_{diag} does not destroy this order (see section III). Furthermore, while $t_\perp > t_c$ destroys the SDW order (leaving the BCDW intact) by disordering the spins on the sites labeled ‘0’ (see section III), a small t_{diag} will have a tendency to restore it, since now each small spin has two neighbors with spins of the same sign and one spin with opposite sign. Thus the experimentally observed strong BCDW and a weak nearly vanishing SDW is exactly what we expect within our theory. In Fig. 17 we give a schematic of the spin arrangement in the α -BEDT-TTF lattice; note that the underlying $x \leftrightarrow y$ symmetry in the isotropic 2D limit implies that there are two degenerate orthogonal 2D BCDW states here.

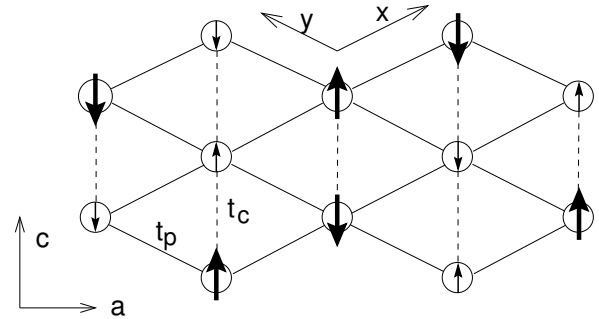


FIG. 17. Schematic view of structure of α -(BEDT-TTF) donor plane from Mori et al.⁷⁶ and Ducasse and Fritsch⁷⁷. The solid lines correspond to stronger interstack t_p hopping integrals, the dotted lines to weaker intrastack t_c hopping integrals. The a and c directions indicated are the crystal axes, and the x and y directions correspond to along the chain and perpendicular to the chains in Fig. 2. The arrangement of the spins in the BCS-DW state is indicated. Any SDW should be weak because of the nearly isotropic 2D nature of the lattice, but nonvanishing because of the nonzero t_c , which becomes t_{diag} in the x - y coordinate system of Fig. 2 (see text).

Since charge ordering in the α -(BEDT-TTF)₂MHg(SCN)₄ has also been discussed by Kino and Fukuyama³⁹, and more recently, by Seo⁷⁸, we should point out that the charge-ordering proposed by these authors is different from that in Fig. 17. Our charge-ordering in Fig. 17 is essentially derived from Fig. 2, where the occupancy scheme is ...1100... along the x -direction and along the diagonals. The charge-ordering found by Kino and Fukuyama, and by Seo, assumes that the ...1010... order dominates over the ...1100... order. Thus the ordering determined by Kino and Fukuyama is within a Hartree-Fock solution to the simple Hubbard model (zero intersite Coulomb interaction and zero e-ph coupling) and consists of a stripe structure with stack occupancies (c-direction in Fig. 17) alternating, *i.e.*, stacks are either completely filled or completely devoid of holes). More recently, Seo has repeated these calculations by incorporating nearest neighbor Coulomb interaction V , but by treating U within the Hartree-Fock approximation and the V within the Hartree approximation. Different stripe structures, including that of Fukuyama and Kino, are found now, but once again, these are derived fundamentally from the occupancy scheme ...1010... As has, however, been pointed out by previous authors^{19,27}, the ...1010... charge ordering for the case of $V = 0$ is an artifact of the Hartree-Fock approximation. Similarly, the Hartree approximation for V also exaggerates the ...1010... order while the Hartree-Fock treatment of the Hubbard term exaggerates the SDW order. This is precisely why these authors find very large magnetic moments in the α -phase materials.

D. κ -(BEDT-TTF)₂X

The deviation from the rectangular lattice is much stronger here³¹. Crystal structure effects are very strong, and as a consequence the lattice is strongly dimerized, with the dimer sites forming an effective triangular lattice³⁹. The strong deviation from the rectangular lattice precludes direct comparisons against our theory. A more elaborate discussion of the spin arrangement will be given elsewhere. Here we only point out that (a) our calculations with the dimerized dimer lattice indicate that very large spin moments are possible when the intra-dimer hopping integrals are large compared to the inter-dimer hopping (see Fig. 15), in qualitative agreement with the observed very large magnetic moment in κ -(BEDT-TTF)₂Cu(CN)₂Cl⁷¹, and (b) each dimer of BEDT-TTF molecules has the cartoon occupancy of 10 or 01 and the ...1100... ordering along one direction and ...1010... ordering along another (see Fig. 2), thereby reducing the spin frustration among the dimer sites forming the triangular lattice. In the absence of this population difference within each dimer cell (and the population difference is a consequence only of dimerization of the dimer lattice) the frustration within the triangular lattice would have severely reduced magnetic moments. We further point out that a pseudo-gap in the spectrum of magnetic excitations has been observed in κ -(BEDT-TTF)₂Cu[N(CN)₂]Br^{79,80} and κ -(BEDT-TTF)₂Cu(NCS)₂⁸⁰, which is in agreement with the dimerization of the dimer lattice, since without the second dimerization there should be no spin gap within the 2D antiferromagnet.

One particular κ -phase material, κ -(BEDT-TTF)₂-Cu₂(CN)₃ merits separate discussion. This material is not antiferromagnetic, and measurement of spin susceptibility due to the BEDT-TTF components exhibits a steep drop below 10 K, suggesting SP-like behavior⁸¹. This behavior is very similar to that in the BETS-based materials, which we discuss below, where we point out that for $\rho = 1/2$, this behavior is expected for the case of large t_{\perp} ($> t_{\perp}^c$).

E. λ -(BETS)₂GaBr_zCl_{4-z} (BETS = BEDT-TSF)

These materials, discovered only recently⁸²⁻⁸⁴, are superconducting for $0 < z \leq 0.8$ and semiconducting for $0.8 < z < 2.0$. Thus the proximity between a semiconducting and a superconducting state that characterizes the TMTSF and the BEDT-TTF is also a characteristic feature of the λ -BETS. In contrast to the TMTSF and the BEDT-TTF systems, however, the semiconducting state in the BETS is *nonmagnetic*, and possesses a spin gap⁸⁵. Magnetic susceptibility studies indicate absence of anisotropy in the susceptibility, and no spin-flop transition (signature of antiferromagnetism) was found down to 10 K, which is close to the maximum supercon-

ducting critical temperature T_c (onset 7.5 K, and even higher in certain samples)⁸². The absence of the SDW is particularly perplexing here in view of the strong two-dimensionality predicted within extended Hückel band calculations⁸⁴.

The lattice structures of the λ -(BETS)₂GaBr_zCl_{4-z} are known⁸². The stacking of the organic donor molecules is very similar to the β -BEDT-TTF systems, *i.e.*, a nearly rectangular lattice with strong intrastack coupling, weaker transverse coupling, and very weak coupling along one diagonal. The nearly rectangular lattice permits comparison with our theory. One interesting feature of the lattice structure is that the intrastack bonds have strengths that are W'SWS, exactly the structure expected for a dimerized dimer lattice. We believe that while the difference between the strong and weak bonds is a crystal structure effect, the further dimerization of the dimer lattice is a consequence of the BCDW instability discussed here.

Hartree-Fock calculations by Seo and Fukuyama⁸⁶ within an anisotropic Hubbard Hamiltonian gave an antiferromagnetic ground state instead of the nonmagnetic state. Since Hartree-Fock calculations overestimate antiferromagnetism, these authors then chose the $U \rightarrow \infty$ limit of Hubbard model to arrive at a dimerized anisotropic 2D Heisenberg spin Hamiltonian, each lattice site of which corresponds to one dimer of the original BETS lattice. The antiferromagnetic-SP boundary within the 2D dimerized Heisenberg spin Hamiltonian has been investigated by Katoh and Imada using QMC simulations⁸⁷. For the longitudinal and transverse exchange integrals derived by Seo and Fukuyama, the QMC calculations still predict the antiferromagnetic structure⁸⁶. Seo and Fukuyama explain the spin gap in λ -BETS by claiming that the second dimerization of the dimer lattice (*i.e.*, intermolecular distances W'SWS, instead of WSWS) takes these systems to the 1D side of the 1D-2D antiferromagnetic-SP boundary, exactly as (TMTTF)₂PF₆, even though the actual transverse hopping integrals are large.

We believe that the problem faced by these authors arises entirely from their effective 1/2-filled band approximation. As seen in Fig. 15, the dimerization of the dimer lattice enhances the SDW in the region of small to intermediate t_{\perp} and therefore cannot be the origin of the spin gap or supposedly 1D behavior. Recall also that (TMTTF)₂PF₆, which is certainly on the 1D side of the 1D-2D boundary, is nonsuperconducting. In contrast, λ -BETS does become superconducting and that too at a T_c that is considerably higher than that in the (TMTSF)₂X, indicating what we believe to be strongly 2D character⁸⁴. We believe that the solution to this puzzle lies in recognizing the $\rho = 1/2$ character of the (BETS)₂X. An essential difference between the effective 1/2-filled band model of Seo and Fukuyama and ours is that within the former, there are only two regions, nearly 1D and 2D, with the spin states as singlet and antiferromagnetic, respectively. Our work indicates that there are three distinct regions,

singlet, antiferromagnet, and singlet again, as a function of increasing t_{\perp} , independent of whether one assumes a 1/4-filled band or an effective 1/2-filled band. We therefore believe that a more natural explanation of the spin gap phase is obtained within our theory, with the singlet ground state in semiconducting BETS not being due to t_{\perp} that is too small, *but due to a t_{\perp} that is too large* ($> t_c$) to give SDW. This would be in agreement with the strong two-dimensionality of these systems^{82,84}. We believe that the same explanation also applies to the κ -(BEDT-TTF)₂Cu₂(CN)₃, discussed in the above. We predict that experiments that can probe charge ordering will find two kinds of BETS molecules with different electronic populations, with greater charge densities on the two BETS molecules that are linked by the W' bond.

VII. CONCLUSIONS AND DISCUSSIONS

Our analyses in the preceding sections have established the surprising conclusions that the strongly interacting, anisotropic 2D 1/4-filled system is a BCDW for all interchain coupling. The BCDW coexists with a SDW—to form a BCDSW²⁴—for small but nonzero t_{\perp} . For the dimerized dimer Hamiltonian, the range of t_{\perp} over which the SDW occurs depends on the strength of the original dimerization and can be large. Nevertheless, at large t_{\perp} the SDW also vanishes. The dominance of the BCDW and the disappearance of the SDW in the large t_{\perp} region is exactly opposite to what happens in the 1/2-filled band.

We have made detailed comparisons between our theory and experiments in the organic CTS. It appears that an understanding of the bond, charge and spin ordering for the family of 2:1 CTS, spanning nearly the entire range from weak t_{\perp} to strong t_{\perp} , can be obtained within our theory. Several recent studies have found evidence for a gap like feature in the spectrum of magnetic excitations even in the SDW phase of the organic CTS^{79,80,88}. The BCSDW and BCDW states are expected to have such a spin gap. The theory also gives a natural explanation for the gap seen in various optical or transport studies on different CTS materials. For example, recent data on the frequency-dependent optical conductivity in the high temperature “metallic” phase of (TMTSF)₂ClO₄ and (TMTSF)₂PF₆ exhibit both zero- and finite-energy modes^{89,90}, with the zero-energy mode having a spectral weight of only about 1 %. Assuming that the (TMTSF)₂X are weakly incommensurate⁸⁹, our BCDW state provides a natural explanation, with the zero-energy mode ascribed to the conductivity of the commensurability defects and the gap mode to the excitation across the BCDW pseudo-gap that persists at high temperature, due to fluctuations associated with low dimensionality. Similarly, evidence for a partial gap has been found in the ¹³C-NMR studies of α -(BEDT-TTF)₂KHg(SCN)₄ in high magnetic fields, in a region

where the system was previously thought to be a metal⁷⁵. It is likely that the conductivity in the so-called metallic phase is due to commensurability defects.

What might be the relation of our BCSDW and BCDW states to organic superconductivity, the mechanism for which remains unclear despite two decades of research? The similarities between the organic and high temperature oxide superconductors have been pointed out in recent years by several research groups^{40,91–94}. One obvious apparent similarity between these two classes of superconductors is the proximity of the SDW to superconductivity. Our studies suggest that superconductivity in the organics is actually occurring at the interface of a Coulomb-induced BCDW that for a range of t_{\perp} coexists with the SDW. Thus the proximity to the SDW is perhaps coincidental. As noted above, the experimental observation of superconductivity in the λ -(BETS)₂GaCl₄ (where no proximate SDW is observed⁸⁵) supports this view. Hence our present work casts doubt on recent spin-fluctuation theories of *organic* superconductivity within the effective 1/2-filled correlated electron model^{95–99}. The implications of this conclusion from the organics for the high T_c materials are unclear, but it is perhaps not irrelevant in this context to point out that evidence for superconductivity within the 2D nearly 1/2-filled Hubbard model, which for large U has strongly AFM behavior, has remained elusive^{100–102}, despite more than a decade of intense research^{51,103,104}.

We suggest that organic superconductivity arises from the pairing of commensurability defects within the BCDW background. For the organic CTS, incommensurability away from 1/4-filling is strongly indicated by (i) the observation of a zero-energy mode in the optical conductivity^{89,90} of (TMTSF)₂PF₆ and (TMTSF)₂ClO₄; (ii) the observation of Fröhlich mode sliding transport in the same materials⁶⁷; and (iii) the observation of a “partially gapped Fermi surface” in the metallic region⁷⁵ of α -(BEDT-TTF)₂KHg(SCN)₄. Extremely interesting results in this context were reported by Komatsu et. al.⁸¹, who showed that the superconductivity in κ -(BEDT-TTF)₂Cu₂(CN)₃ was due to a subtle change in the valence state of the Cu. The pure κ -phase material is a semiconductor with the Cu valence of +1. According to the authors of Ref. 81, the superconducting phase corresponds to a different material (κ' in the authors' notation) in which some of the Cu (several hundred ppm) have acquired valency 2+. This was confirmed from ESR studies. The increase in Cu valency decreases the overall negative charge on the anion, and therefore the overall positive charge on the cation, providing a weak incommensurability that appears to be essential for superconductivity⁸¹.

Also suggestive are the striking similarities between the BCSDW/BCDW states and several other states reached within theoretical models that in principle can lead to superconductivity. First, as we have noted previously, the BCSDW and the BCDW states are very similar to the “paired electron crystal” (as opposed to the monatomic

Wigner crystal) found by Moulopoulos and Ashcroft for the intermediate density electron gas⁵⁸. Superconductivity near the “melting” transition of the paired electron crystal has been conjectured by a number of authors in the past^{105–108}, even before the discovery of high T_c superconductivity. Second, the commensurate BCDW is qualitatively similar to a “negative U - positive V” effective 1/2-filled extended Hubbard model, with the effective lattice sites consisting of (a) the “occupied” pair (‘1–1’) of nearest neighbor sites, and (b) the “unoccupied” pair (‘0–0’) of nearest neighbor sites, in Fig. 1(c). Within this scenario, there is an effective attraction between the carriers on the “occupied” pair of dimer sites, but an effective repulsion between two pairs of occupied dimers. For models of this type, it is known that diagonal and off-diagonal long-range order can in principle coexist slightly away from commensurate filling^{109–111}. Third, Imada has studied¹¹² a 2D spin-Peierls state (not possible in the monatomic 1/2-filled band) in which each composite site is again a dimer, with the dimer sites now having occupancies ‘10’ and ‘01’ (see Fig. 2(b) and note that the bonds between a ‘10’ and ‘01’ and between a ‘01’ and a ‘10’ are different, giving rise to a spin-Peierls-like behavior). His numerical simulations find evidence for superconductivity in the hypothetical doped 2D spin-Peierls state¹¹². Fourth, Emery, Fradkin, and Kivelson have recently suggested⁵⁰ that superconductivity can exist for incommensurate fillings in models that support stripe phases and in which a spin gap is present. Since the analysis in Ref. 50 does not make direct contact with an initial microscopic Hamiltonian, but rather posits the form of the effective Hamiltonian in the vicinity of an unpinned stripe phase, it is not possible immediately to make detailed comparisons with our results. We can, however, make two comments. First, Ref. 50 reflects the widespread belief that models within which a spin gap persists in the doped state are strong candidates for a microscopic theory of correlated superconductivity. Our preliminary numerical evidence suggests that both the BCDW and the BCSDW will continue to have a spin gap when doped; further work is in progress to confirm this. Second, regarding the attractive possibility that our BCSDW/BCDW state provides the background charge order within which commensurability defects may pair to form a superconducting state, we note that the occupancy schemes in Fig. 1(c) and Fig. 2(a) and (b) resemble intersecting stripes, where each stripe is obtained by connecting the ‘1–1’ bonds along the x- and x+y (−x+y) directions.

The possible BCSDW/BCDW to superconductor transition in the organic CTS clearly merits (and requires!) further study. We close our present discussion of this topic with comments on three important open issues: (i) the possible mechanism for superconducting pairing; (ii) the problem of phase separation; and (iii) the symmetry of the order parameter.

First, the possible mechanism for pairing of commensurability defects within the 2D BCDW can be visualized

most simply in the rigid bond limit, nearest neighbor bonds retain their individual distortions independent of the occupancies of the sites linked by these bonds. The commensurate BCDW in this limit can be viewed as consisting of “quasimolecules”, where each quasimolecule is a “1–1” dimer. If two holes are now removed from the system, it is energetically preferable to destroy one “quasichemical bond,” thereby creating an intersite (small) bipolaron, as opposed to destroying two bonds and creating two polarons. Thus, within the W’SWS structure ($t_S > t_W > t_W'$), each W’ bond acts as a “negative-U” center in the rigid bond limit. It is of course highly unlikely that superconductivity can be obtained, at least at the experimental T_c , due to condensation of small bipolarons¹¹⁰, so this might appear to present a serious problem to this proposed mechanism. In fact, when we go beyond the oversimplified rigid bond limit to our full model that correctly reflects the cooperation between e-e and e-ph interactions in the 1/4-filled band, we find that the actual commensurability defects are more like the extended, “resonant” (and therefore mobile) bipolarons that are indeed candidates for explaining superconductivity in strongly correlated systems^{110,111}. To understand this in detail, consider again the weakly incommensurate BCDW, starting from the 1D limit, but now with the e-ph interactions included. Below the $4k_F$ transition temperature T_{4k_F} , but above the $2k_F$ transition temperature T_{2k_F} , incommensurability leads to *fractionally charged* solitons with charge $e/2$ and each vacancy creates two such defects^{113,114}. Previous work has assumed that the soliton charge remains $e/2$ even below the $2k_F$ transition, which implies that two vacancies create four such defects¹¹⁴. However, Ref. 114 assumes that the site charge density remains uniform even below the 1D $2k_F$ SP (dimerization of the dimer lattice) transition, which is precisely what we have shown here not to be the case. Indeed, as a consequence of this spatial charge inhomogeneity (charge ordering), the “solitons” now acquire integer charge (*i.e.*, two fractionally charged solitons bind to give a single soliton with charge $+e$), as we have shown explicitly elsewhere¹¹⁵. A pair of added vacancies within the 1D BCDW below T_{2k_F} therefore creates (only) two solitons. In the strictly 1D limit, these do not bind, but with increasing t_\perp , one expects binding to a *large* bipolaron. The source of this binding is precisely the same as the source of soliton confinement in coupled chains of polyacetylene¹: in the region between the two defect centers the phase relationships between the BCDW’s on neighboring chains is different from the preferred one (*viz.*, π), and therefore a large separation between the defect centers would increase the energy (linearly with increasing separation). There exists therefore a *space-dependent* interaction between the polarons, which is repulsive at short range but attractive at some (t_\perp -dependent) intermediate range. The bipolaron size, as well as its dimensionality, depends on t_\perp (as well as on U and V). There is currently limited analysis of 2D large bipolarons in the strongly correlated limit, although

some results suggest that these can indeed be mobile¹¹¹. Within this scenario, superconductivity occurs due to the condensation of these large bipolarons, which is *not* precluded by the theoretical analysis of Ref. 110. Resolving the question of whether static distortion is sufficient, or whether dynamical phonons will have to be included, will require further work.

Second, in many existing models of superconducting pairing involving correlated electrons, the interactions that bind two particles also lead to phase separation, since the attraction producing pairing does not saturate. Perhaps the best known example of this is the t-J model^{103,116} away from 1/2-filling. In contrast, within any “negative U” model there does exist a saturation in this attraction (since a single site can at most have two electrons), and the analogy between our BCDW model and the effective 1/2-filled “negative U – positive V” case suggests that phase separation will also not occur here. Further, the immediately previous discussion of the proposed binding mechanism makes clear that with small but macroscopic (say, 1%) concentration of commensurability defects, there is no particular energetic advantage in creating additional polarons or bipolarons proximate to the original bipolaron (in contrast to, say, the t-J model, where there *is* such an energetic advantage).

Third, what symmetry do we expect for the superconducting order parameter in our model? This is clearly a challenging issue, particularly since even with the *same* BCDW background the pairing symmetry in the highly anisotropic TMTSF *might* be different from that in the more two-dimensional BEDT-TTF and BETS. Several recent experiments have presented evidence consistent with nodes in the superconducting gap function in the BEDT-TTF^{117–120}. This is reminiscent of d-wave symmetry of the superconducting order parameter in the high temperature copper oxide based superconductors. On the other hand, Lee et al. have recently presented evidence^{121,122} suggesting that a spin triplet p-wave pairing is necessary to explain data in (TMTSF)₂PF₆, where the upper critical field H_{c2} shows no saturation with the field in the plane of the organic molecules and exceeds the Pauli paramagnetic (“Clogston”) limit expected to hold for singlet superconductors¹²¹ and the temperature dependent Knight shift measurements of ⁷⁷Se show that the spin susceptibility remains unaltered through the superconducting T_c¹²². Within the continuum RG theories^{16,17} triplet superconductivity does indeed occur proximate to the SDW. However, within the discrete extended Hubbard model, triplet superconductivity occurs within a very narrow region of the the “positive U – negative V” sector of the U – V phase diagram, bounded by the SDW phase and a phase segregated phase⁵⁶. Triplet pairing thus will not only require a change in sign of the nearest neighbor Coulomb interaction within our original Hamiltonian of Eq. (1), but will also occur for a very narrow critical range of this parameter. But to resolve definitively the issue of the symmetry of the order parameter within our model will be a non-trivial task, as

the consequences of the interplay between e-e and e-ph interactions, as well as the effects of anisotropy, must be properly understood.

In conclusion, we have shown that the interacting 2D 1/4-filled band has a persistent insulating BCDW ground state for all anisotropies. We believe that such a state can appropriately describe the insulating state proximate to organic superconductivity in several different classes of materials. We have further pointed out that in the the weakly incommensurate region our model has similarities with four different models of superconductivity. More quantitative studies of the relationship between the BCDW/BCSDW states and organic superconductivity are currently in progress.

VIII. ACKNOWLEDGMENTS

We thank Jim Gubernatis and Shiwei Zhang for discussions regarding the CPMC method, Eduardo Fradkin and Philip Phillips for discussions of their recent theoretical results, and Stuart Brown, Paul Chaikin, and Andrew Schwarz for discussions of their experiments. Work at the University of Illinois was supported in part by the grants NSF-DMR-97-12765 and NSF-GER-93-54978 and by an allocation of supercomputer time through the NRAC program of the NCSA.

APPENDIX

As discussed in section V.B, the proper boundary condition for the numerical evaluation of the electronic energy gained upon bond or site distortion in $\rho = 1/2$ involves finite $N \times M$ lattices with $N = 8n$. This requires the number of electrons per chain to be $4n$, and it is known that in 1D periodic *undistorted* rings with $\rho \neq 1$, the ground state has overall spin $S = 1$ instead of 0 for any nonzero U .

The spin of the ground state of the distorted periodic ring depends on its size and the magnitude of the Hubbard U . For the values of the correlation parameters and bond distortion parameter in Fig. 9, the ground state in the $N = 8$ distorted periodic ring has $S = 1$, while the $N = 16$ ground state has $S = 0$. Thus the ΔE_0 in Fig. 9 for nonzero e-e interaction corresponds to ΔE_{TT} (*i.e.*, the energy gained by the triplet state upon bond distortion) for $N = 8$, and to ΔE_{TS} (undistorted state in $S = 1$, distorted state in $S = 0$) for $N = 16$. Whether or not the comparisons of the zero and nonzero t_{\perp} are then meaningful is an important question. We present here the detailed results of three different sets of calculations, each of which indicates that our interpretation of the results of Fig. 9 (viz., strong tendency of the interacting 1/4-filled lattice to distort at arbitrary t_{\perp}) is correct.

First, we have calculated the exact ground states of the 8×2 lattice for t_{\perp} as small as 0.01. In Table A we have

given the $S = 0$ and $S = 1$ energies of the 8×2 lattice for $U = 6$ and $V = 1$, for three small values of t_{\perp} . As might be anticipated from Fig. 5, the coupled chain system is in the $S = 0$ state for *both* zero and nonzero bond distortion for the smallest nonzero t_{\perp} . The important point now is that instead of choosing the single isolated chain as the standard in Fig. 9, we could have also chosen the coupled chain system with $t_{\perp} = 0.01$ as the standard, provided the distortion of the $t_{\perp} = 0.01$ lattice is also unconditional. Even if the nesting ideas were valid, we believe that the coupled chain system with $t_{\perp} = 0.01$ is unconditionally distorted and then the results in Table A clearly show that ΔE increases with further increase in t_{\perp} , indicating enhanced distortion relative to $t_{\perp} = 0.01$. The error bars in the CPMC calculations prevent us from performing similar calculations for the 8×6 or the 16×6 lattices, but the overall similarities in the (a) occupancies of the one-electron levels for nonzero t_{\perp} and (b) ΔE behavior, especially in the region $t_{\perp} \leq 0.4$, preclude different behavior at small nonzero t_{\perp} .

t_{\perp}	undistorted		2k _F distortion	
	S=0	S=1	S=0	S=1
0.01	-9.335651	-9.335637	-9.352522	-9.352228
0.025	-9.337570	-9.336944	-9.354380	-9.353739
0.05	-9.344122	-9.341546	-9.361083	-9.358425

Table A: The $S=0$ and $S=1$ energies of the 8×2 undistorted and $2k_F$ bond-distorted lattice for $U = 6$ and $V = 1$. The lowest energy is $S=0$ for both undistorted and distorted cases.

We performed a second set of calculations for the 8×2 lattice for very small values of U (with $V = 0$). Note that if the persistent distortion implied in Fig. 9 were merely due to our choosing the wrong reference point $t_{\perp} = 0$ (since exactly at this point $\Delta E_0 = \Delta E_{TT}$), an apparently enhanced distortion for nonzero t_{\perp} should occur for *all* nonzero U (since the single chain is $S = 1$ for all nonzero U , while the coupled chain system has $S = 0$ for all nonzero t_{\perp} and U). On the other hand, if the results in Fig. 9 are due to the confinement effect discussed in section III.D, then enhanced/persistent distortion should occur only *above a threshold e-e interaction*: for weak e-e interaction the behavior should resemble that of the non-interacting lattice (with enhanced or persistent distortion occurring for a small range of t_{\perp} near $t_{\perp} = 0$). We show here the results of calculations at small U for *site* distortion (as opposed to bond distortion), since we also report calculations for very large U below, and the bond distortion pattern (the magnitude of r_{4k_F}) is U -dependent, but the site distortion pattern is not. The distorted lattice here has site energies $+\epsilon, +\epsilon, -\epsilon, -\epsilon$ (with $\epsilon = 0.1$) over four consecutive sites, and a π -phase shift between the two periodic rings. Since the $2k_F$ CDW has a synergistic coexistence with both the $r_{4k_F} = 0$ BOW (Fig. 2(a)) and the $r_{4k_F} \neq 0$ BOW (Fig. 2(b))²⁷ a persistent CDW also implies persistent BOW; we have confirmed this by calculating the expectation values of the bond orders. In

Fig. 18(a) we show the ΔE behavior as a function of t_{\perp} for both $U = 0.5$ and $U = 1$. Decreasing ΔE with t_{\perp} is a clear signature that the tendency to distortion here *decreases* with increasing two dimensionality, since confinement at these small U is not sufficient to give persistent distortion. Even though these calculations are with fixed site energies, the expectation values of the charge densities depend on t_{\perp} , and our calculated CDW amplitudes decrease with t_{\perp} , as expected from Fig. 18(a). This behavior is exactly opposite to that in Fig. 10(b), indicating again a decrease in distortion with t_{\perp} at small U . Finally, we emphasize that similar calculations have also been done with fixed $2k_F$ bond distortion, and once again we observe decreasing ΔE and CDW amplitude with increasing t_{\perp} .

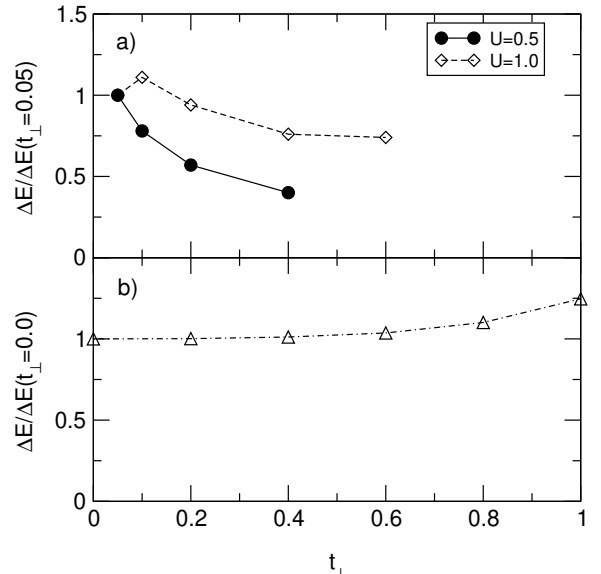


FIG. 18. (a) ΔE vs. t_{\perp} for the 8×2 lattice at small U (normalized to the value at $t_{\perp} = 0.05$). Note the decrease in the ΔE . (b) $\Delta E / \Delta E_0$ vs. t_{\perp} for the 8×2 lattice at $U = 100$.

We performed a third set of calculations with very large $U = 100$, again with the same site distorted lattice but now with $\epsilon = 0.2$, since at this very large U , the energy gained upon distortion for $\epsilon = 0.1$ is very small. The resultant BOW here has strong $4k_F$ component ($r_{4k_F} \neq 0$), and this is why the distorted lattice was chosen to be the $2k_F$ CDW in this and the above calculations, such that meaningful comparisons between these extreme cases can be made. At this large U , the energy difference between $S = 0$ and $S = 1$ states is negligible. For example, for the 1D 8-site periodic ring ΔE_{SS} (electronic energy gained in the $S = 0$ subspace, with both undistorted and distorted states in $S = 0$) = 0.06222, while ΔE_{TT} (electronic energy gained in the $S = 1$ subspace, with both undistorted and distorted states in $S = 1$) = 0.06224. Fig. 18(b) shows the ΔE behavior as a function of t_{\perp} (with $\epsilon = 0.2$ now). An enhanced CDW (and therefore BOW) is seen from as a function of t_{\perp} , where the singlet and triplet data points at $t_{\perp} = 0$ are the same. As

seen in Fig. 18(b), the ΔE for nonzero t_{\perp} is weakly enhanced now even when compared to ΔE_{SS} at $t_{\perp} = 0$. Once again, the behavior of the CDW amplitude is in complete agreement with the prediction from Fig. 18(b), viz., a weak enhancement of the CDW amplitude with t_{\perp} .

Considering the above three different sets of results, we therefore conclude that the results in Fig. 9, Fig. 10(b) and Fig. 14 are not artifacts, and the persistent distortion is real and a true confinement effect, as would also be expected from the “variational” arguments of Section III.D.

²³ H.H. Lin, L. Balents and M.P.A. Fisher, Phys. Rev. B **56**, 6569 (1997).

²⁴ S. Mazumdar, S. Ramasesha, R. Torsten Clay and D.K. Campbell, Phys. Rev. Lett. **82**, 1522 (1999).

²⁵ An abbreviated discussion of the evolution of the BCSDW into the BCDW for large t_{\perp} can be found in S. Mazumdar, R. T. Clay, and D. K. Campbell, cond-mat/9910164.

²⁶ K.C. Ung, S. Mazumdar and D.K. Campbell, Solid St. Commun. **85**, 917 (1993).

²⁷ K.C. Ung, S. Mazumdar and D. Toussaint, Phys. Rev. Lett. **73**, 2603 (1994).

²⁸ J. Riera and D. Poilblanc, Phys. Rev. B **59**, 2667 (1999).

²⁹ T. Holstein, Ann. Phys. **8**, 325 (1959).

³⁰ D. Jerome and H. Schulz, Adv. in Phys. **31**, 299 (1982).

³¹ T. Ishiguro, K. Yamaji and G. Saito, *Organic Superconductors*, 2nd Ed., Springer Series in Solid State Sciences, Vol. 88 (Springer Verlag, Berlin, 1998).

³² D. Jerome, Science **252**, 1509 (1991).

³³ P.W. Anderson, Phys. Rev. Lett. **67**, 3844 (1991).

³⁴ D.G. Clarke, S.P. Strong and P.W. Anderson, Phys. Rev. Lett. **73**, 1007 (1994).

³⁵ Given that the issue of confinement in interacting electron systems has been hotly debated, it is pertinent to emphasize that we use this expression in a considerably narrower sense than has sometimes been used in the literature. Our interest lies strictly in the interacting 1/4-filled band case, and it is not being implied that the effect discussed here applies to other bandfillings.

³⁶ J.P. Pouget and S. Ravy, J. Physique I, **6**, 1501 (1996).

³⁷ C. Bourbonnais, Synth. Metals **84**, 19 (1997).

³⁸ K. Kanoda, Hyperfine Interactions, **104**, 235 (1997).

³⁹ H. Kino and H. Fukuyama, J. Phys. Soc. Jpn. **65**, 2158 (1996).

⁴⁰ R.H. McKenzie, Comments Cond. Mat. Phys. **18**, 309 (1998).

⁴¹ P.M. Chaikin, J. Phys. I. (France) **6**, 1875 (1996).

⁴² L.P. Gor'kov, J. Phys. I. (France) **6**, 1697 (1996).

⁴³ In all cases X are inorganic anions that play only indirect roles in accepting electrons from the organic cations, and do not have any active role in charge transport, although they do influence the magnitudes of the interchain hopping integrals.

⁴⁴ J.P. Pouget and S. Ravy, Synth. Metals, **85**, 1523 (1997).

⁴⁵ S. Kagoshima, Y. Saso, M. Maesato, R. Kondo and T. Hasegawa, Solid St. Commun. **110**, 479 (1999).

⁴⁶ The BCSDW has also been found in 1D Hartree-Fock calculations within the dimerized dimer lattice, see N. Kobayashi and M. Ogata, J. Phys. Soc. Jpn. **66** 3356 (1997). The SDW component here, however, is an artifact of the Hartree-Fock approximation as in 1D the spin couplings are necessarily singlet.

⁴⁷ The underlying $x \leftrightarrow y$ symmetry in the isotropic 2D limit implies that there are two degenerate orthogonal 2D BCDW states for $t_{\perp} = t$.

⁴⁸ R. T. Clay, A. W. Sandvik, and D. K. Campbell, Phys. Rev. B **59**, 4665 (1999).

⁴⁹ M. Nakamura, cond-mat/9909277.

⁵⁰ V. J. Emery, E. Fradkin, and S. A. Kivelson, cond-mat/0001077.

⁵¹ For two recent articles claiming to find d-wave super-

- ¹ D. Baeriswyl, D.K. Campbell and S. Mazumdar in *Conjugated Conducting Polymers*, edited by H. Kiess (Springer Verlag, Berlin, 1992) pp. 7 - 133.
- ² A.J. Heeger, S. Kivelson, R.J. Schrieffer and W.-P. Su, Rev. Mod. Phys., **60**, 781 (1988).
- ³ S.N. Dixit and S. Mazumdar, Phys. Rev. B**29**, 1824 (1984). S. Mazumdar and D.K. Campbell, Phys. Rev. Lett. **55**, 2067 (1985).
- ⁴ S. Kivelson, Phys. Rev. B **28**, 2653 (1983).
- ⁵ W.-P. Su, Solid St. Commun. **48**, 479 (1983).
- ⁶ J.E. Hirsch, Phys. Rev. Lett. **53**, 2327 (1984).
- ⁷ E. Manousakis, Rev. Mod. Phys. **63**, 1 (1991) and references therein.
- ⁸ S. Mazumdar Phys. Rev. B **36**, 7190 (1987) and *ibid*, **39**, 12324 (1989).
- ⁹ F.C. Zhang and P. Prelovsek, Phys. Rev. B **37**, 1569 (1988).
- ¹⁰ S. Tang and J.E. Hirsch, Phys. Rev. B **37**, 9546 (1987) and *ibid*, 12327 (1989).
- ¹¹ A.W. Sandvik, Phys. Rev. Lett. **83**, 3069 (1999).
- ¹² I. Affleck and B. Halperin, J. Phys. A **29**, 2627 (1996).
- ¹³ Z. Wang, Phys. Rev. Lett. **78**, 126 (1997).
- ¹⁴ E. Dagotto and T.M. Rice, Science, **271**, 618 (1996) and references therein.
- ¹⁵ F.D.M. Haldane, Phys. Lett. **93A**, 464 (1983).
- ¹⁶ J. Solyom, Adv. Phys. **28**, 201 (1979).
- ¹⁷ V.J. Emery in *Highly Conducting One-Dimensional Solids*, edited by J.T. Devreese et al., (Plenum, N.Y. 1979).
- ¹⁸ J. Voit, Rep. Progr. Phys. **58**, 977 (1995).
- ¹⁹ J.E. Hirsch and D.J. Scalapino, Phys. Rev. B **27**, 7169 (1983) and *ibid* **29**, 5554 (1984).
- ²⁰ S. Mazumdar, S.N. Dixit and A.N. Bloch, Phys. Rev. B **30**, 4842 (1984).
- ²¹ We exclude from our discussions the extensive work on doped 2- and 4-leg ladder systems. It is not clear currently whether or not these results are relevant for the true 2D lattice.
- ²² A true metallic phase may not be obtained because of disorder effects, but this is a different issue that is unrelated to the question of the existence of density waves, and is hence ignored here.

conductivity within (different) strong-coupling approximation to the 2D Hubbard model, see T. Stanescu, I. Martin, and P. Phillips, cond-mat/0001254, and Th. Maier, M. Jarrell, Th. Pruschke, and J. Keller, cond-mat/0002352.

⁵² J. Hubbard, Phys. Rev. B **17**, 494 (1978).

⁵³ D.J. Klein and W.A. Seitz, Phys. Rev. B **10**, 3217 (1974).

⁵⁴ P. Jordan and E. Wigner, Z. Phys. **47**, 631 (1928).

⁵⁵ J.D. Johnson and B. McCoy, Phys. Rev. A **6**, 1613 (1972).

⁵⁶ H. Q. Lin, E. R. Gagliano, D. K. Campbell, E. H. Fradkin, and J. E. Gubernatis, in *The Hubbard Model*, edited by D. Baeriswyl *et al.* (Plenum Press, New York, 1995), pp. 316 – 336.

⁵⁷ F.D.M. Haldane, Phys. Rev. Lett. **45**, 1358 (1980); J. Phys. C **14**, 2585 (1981).

⁵⁸ K. Mouloupoulos and N. Ashcroft, Phys. Rev. B **48** 11646 (1993).

⁵⁹ S. Zhang, J. Carlson and J.E. Gubernatis, Phys. Rev. Lett. **74**, 3652 (1995); Phys. Rev. B **55**, 7464 (1997).

⁶⁰ M. Guerrero, J.E. Gubernatis and S. Zhang, Phys. Rev. B **57**, 11980 (1998).

⁶¹ S. Mazumdar, D. Campbell, R.T. Clay and S. Ramasesha, Phys. Rev. Lett. **82**, 2411 (1999).

⁶² B. Domoulin, C. Bourbonnais, S. Ravy, J.P. Pouget and C. Coulon, Phys. Rev. Lett. **76**, 1360 (1996).

⁶³ D.S. Chow, F. Zamborzsky, B. Alavi, D.J. Tantillo, A. Baur, C.A. Merlic and S.E. Brown, “Charge ordering in the TMTTF family of molecular conductors,” preprint (2000).

⁶⁴ C. Coulon, P. Delhaes, S. Flandrois, R. Lagnier, E. Bonjour, J.M. Fabre, J. Physique **43**, 1059 (1982).

⁶⁵ S.S.P. Parkin, J.C. Scott, J.B. Torrance and E.M. Engler, J. Physique Colloque, **44**, C-3, 1111 (1983).

⁶⁶ In order to explain the “purely electronic CDW”, Kobayashi *et al.*, in a 1D calculation have suggested that the transition to the ...1100... CDW is driven by a second neighbor intra-chain Coulomb interaction V_2 [N. Kobayashi *et al.*, J. Phys. Soc. Jpn. **67**, 1098 (1998)]. The synergic coexistence of the BOW and the CDW found by us indicates that a BOW must exist even in this case.

⁶⁷ G. Grüner, Rev. Mod. Phys. **66**, 1 (1994) and references therein.

⁶⁸ T. Sasaki and N. Toyota, Synth. Metals, **70**, 849 (1995).

⁶⁹ F.L. Pratt, T. Sasaki, N. Toyota and K. Nagamine, Phys. Rev. Lett. **74**, 3892 (1995).

⁷⁰ P. Wzietek, F. Creuzet, C. Bourbonnais, D. Jerome, K. Bechgaard and P. Batail, J. Physique I **3**, 171 (1993).

⁷¹ K. Miyagawa, A. Kawamoto, Y. Nakazawa and K. Kanoda, Phys. Rev. Lett. **75**, 1174 (1995).

⁷² K. Miyagawa, A. Kawamoto and K. Kanoda, Phys. Rev. B **56**, R8487 (1997).

⁷³ N. Harrison, Phys. Rev. Lett. **83**, 1395 (1999).

⁷⁴ N. Biskup, J.A.A.J. Perenboom, J.S. Brooks and J.S. Qualls, Solid St. Commun. **107**, 503 (1998).

⁷⁵ P.L. Kuhns, J.S. Brooks, T. Caldwell, W.G. Moulton, A.P. Reyes, N. Biskup, A.M. Kini, J.A. Schlueter, H.H. Wang, U. Geiser and J.M. Williams, Solid St. Commun. **109**, 637 (1999).

⁷⁶ H. Mori, S. Tanaka, M. Oshima, G. Saito, T. Mori, Y. Maruyama, and H. Inokuchi, Bull. Chem. Soc. Jpn. **63**, 2183 (1990).

⁷⁷ L. Ducasse and A. Fritsch, Solid St. Commun. **91**, 201 (1994).

⁷⁸ H. Seo, cond-mat/9911329.

⁷⁹ H. Mayaffre, P. Wzietek, D. Jerome, C. Lenoir and P. Batail, Phys. Rev. Lett. **75**, 4122 (1995).

⁸⁰ A. Kawamoto, K. Miyagawa, Y. Nakazawa and K. Kanoda, Phys. Rev. Lett. **74**, 3455 (1995).

⁸¹ T. Komatsu, N. Matsukawa, T. Inoue, and G. Saito, J. Phys. Soc. Jpn. **65**, 1340 (1996).

⁸² H. Kobayashi, T. Udagawa, H. Tomita, K. Bun, T. Naito and A. Kobayashi, Chem. Lett., 1559 (1993).

⁸³ H. Tanaka, A. Kobayashi, T. Saito, K. Kawano, T. Naito and H. Kobayashi, Adv. Mater. **8**, 812 (1996).

⁸⁴ L.K. Montgomery, T. Burgin, J.C. Huffman, J. Ren, and M.-H. Whangbo, Physics C **219**, 490 (1994).

⁸⁵ H. Kobayashi, H. Akutsu, E. Arai, H. Tanaka and A. Kobayashi, Phys. Rev. B **56**, R8526 (1997).

⁸⁶ H. Seo and H. Fukuyama, J. Phys. Soc. Jpn. **66**, 3352 (1997).

⁸⁷ N. Katoh and M. Imada, J. Phys. Soc. Jpn. **63**, 4529 (1994); *ibid*, **64**, 1437 (1995).

⁸⁸ Y. Nakazawa and K. Kanoda, Phys. Rev. B **60**, 4263 (1999).

⁸⁹ A. Schwartz, M. Dressel, G. Grüner, V. Vescoli, L. Degiorgi and T. Giamarchi, Phys. Rev. B **58**, 1261, (1998).

⁹⁰ V. Vescoli, L. Degiorgi, W. Henderson, G. Grüner, K.P. Starkey and L.K. Montgomery, Science **281** 1181 (1998).

⁹¹ S. Mazumdar, in *Interacting Electrons in Reduced Dimensions*, eds. D. Baeriswyl and D.K. Campbell, NATO ASI Series B, Vol. 213 (Plenum, NY, 1989), pp. 315 - 329.

⁹² R.L. Greene in *Organic Superconductivity*, eds. V. Kresin and W.A. Little, Plenum, N.Y. (1990), pp. 7 – 13.

⁹³ Y.J. Uemura, L.P. Le, G.M. Luke, B.J. Sternlieb, J.H. Brewer, T.M. Riseman, G. Saito and H. Yamochi, in reference 89, pp. 23 – 29.

⁹⁴ B. Brandow, Phys. Rep. **296**, 1 (1998).

⁹⁵ H. Kondo and T. Moriya, J. Phys. Condens. Matter **11**, L363 (1999).

⁹⁶ H. Kino and H. Kontani, J. Phys. Soc. Jpn., **67**, 3691 (1998).

⁹⁷ J. Schmalian, Phys. Rev. Lett. **81**, 4232 (1998).

⁹⁸ M. Vojta and E. Dagotto, Phys. Rev. B **59**, R713 (1999).

⁹⁹ K. Kuroki and H. Aoki, Phys. Rev. B **60**, 3060 (1999).

¹⁰⁰ S. Zhang, J. Carlson and J.E. Gubernatis, Phys. Rev. Lett. **78**, 4486 (1997).

¹⁰¹ M. Guerrero, G. Ortiz and J.E. Gubernatis, Phys. Rev. B **59**, 1706 (1999).

¹⁰² C.T. Shih, Y.C. Chen, H.Q. Lin and T.K. Lee, Phys. Rev. Lett. **81**, 1294 (1998).

¹⁰³ E. Dagotto, Rev. Mod. Phys. **66**, 763 (1994).

¹⁰⁴ D.J. Scalapino, Phys. Rep. **250**, 330 (1995). See also, J. Low Temp. Phys. **117**, 179 (1999).

¹⁰⁵ G.V. Chester, Phys. Rev. A **2**, 256 (1970).

¹⁰⁶ A.F. Andreev in *Progress in Low Temperature Physics*, edited by D.G. Brewer (North Holland, Amsterdam, 1982), Vol. VIII.

¹⁰⁷ D. Nelson and M.E. Fisher, Phys. Rev. Lett. **32**, 1350 (1974).

¹⁰⁸ A.J. Leggett, Phys. Rev. Lett. **25**, 1543 (1970).

¹⁰⁹ A.S. Alexandrov and J. Ranninger, Phys. Rev. B **23**, 1796

(1981); S. Robaskiewicz, R. Micnas and K.A. Chao, Phys. Rev. B **23**, 1447 (1981). Note that these two papers deal with the negative U Hubbard model, which leads to superconductivity via a Bose condensation of small bipolarons. As noted in Ref. 110, this mechanism is unlikely to apply to the high temperature superconductors. We stress that the effective "negative U, positive V" model we envisage here is quite different from the standard "negative U" model in that any bipolarons are expected to be quite extended and thus substantially more mobile. See Refs. 111 for more details. Clearly this issue requires further study.

¹¹⁰ B.K. Chakraverty, J. Ranninger and D. Feinberg, Phys. Rev. Lett. **81**, 433 (1998).

¹¹¹ S. Aubry, p. 217 in *Polarons and Bipolarons in High- T_c Superconductors and Related Materials*, edited by E. K. H. Salje, A. S. Alexandrov, and W. Y. Liang (Cambridge University Press, Cambridge, 1995); L. Proville and S. Aubry, Eur. Phys. J. B **11**, 41 (1999); L. Proville and S. Aubry, Eur. Phys. J. B (to appear).

¹¹² M. Imada, J. Phys. Soc. Jpn. **60**, 1877 (1991); Phys. Rev. B **48** 550 (1993). Note that in the effective spin-Peierls model related to our incommensurate BCDW state, we do not expect nearest neighbor occupancy of defect pairs, as the weak confinement effects arising from the distorted lattice will allow spatially extended paired states.

¹¹³ M.J. Rice and E.J. Mele, Phys. Rev. B **25**, 1339 (1982).

¹¹⁴ S.C. Zhang, S. Kivelson and A.S. Goldhaber, Phys. Rev. Lett. **58**, 2134 (1987).

¹¹⁵ R.T. Clay, S. Mazumdar and D.K. Campbell, unpublished.

¹¹⁶ S.A. Kivelson, V.J. Emery and H.Q. Lin, Phys. Rev. B **42**, 6523 (1990).

¹¹⁷ S.M. De Soto, C.P. Slichter, A.M. Kini, H.H. Wang, U. Geiser and J.M. Williams, Phys. Rev. B **52**, 10364 (1995).

¹¹⁸ Y. Nakazawa and K. Kanoda, Phys. Rev. B **55**, R8670 (1997).

¹¹⁹ S. Belin, K. Behnia and A. Deluzet, Phys. Rev. Lett. **81**, 4728 (1998).

¹²⁰ J.M. Schrama, E. Rzepniewski, R.S. Edwards, J. Singleton, A. Ardavan, M. Kurmoo and P. Day, Phys. Rev. Lett. **83**, 3041 (1999).

¹²¹ I.J. Lee, M.J. Naughton, G.M. Danner and P.M. Chaikin, Phys. Rev. Lett. **78**, 3555 (1997).

¹²² I.J. Lee, D.S. Chow, W.G. Clark, J. Strouse, M.J. Naughton, P.M. Chaikin and S.E. Brown, cond-mat/0001332.